Non-trivial dynamics in a model of glial membrane voltage driven by open potassium pores

Predrag Janjic[1]✉, Dimitar Solev[1], Ljupco Kocarev[1]

[1]Laboratory for Complex Systems and Networks, Research Centre for Computer Science and Information Technologies, Macedonian Academy of Sciences and Arts, Skopje, North Macedonia

✉predrag.a.janjic@gmail.com

Abstract - Despite the molecular evidence that close to linear steady-state current-voltage relationship in mammalian astrocytes reflects a total current resulting from more than one differently regulated K^+ conductances, detailed ODE models of membrane voltage V_m incorporating multiple conductances are still lacking. Repeated experimental results of deregulated expressions of major K^+ channels in glia, Kir4.1, in models of neurodegenerative disease, as well as their altered rectification when assembling heteromeric Kir4.1/Kir5.1 channels have motivated us to attempt a detailed model incorporating the weaker potassium K2P-TREK1 current, in addition to Kir4.1, and study the stability of the resting state V_r. The main question is whether with a deregulated Kir conductivity the nominal resting state V_r remains stable, and the cell retains a *potassium electrode* behavior with V_m following E_K. The minimal 2-dimensional model near V_r showed that certain alterations of Kir4.1 current may result in multistability of V_m if the model incorporates the typically observed K^+currents - Kir, K2P, and non-specific potassium leak. More specifically, a decrease or loss of outward Kir4.1 conductance (turning the channels into inwardly rectifying) introduces instability of V_r, near E_K. That happens through robustly observed fold bifurcation giving birth to a much more depolarized second, stable resting state $V_{dr} > -10\ mV$. Realistic time series were used to perturb the membrane model, from recordings at the glial membrane during electrographic seizures. Simulations of the perturbed system by constant currents through gap-junctions and transient seizure-like discharges as local field potentials led to depolarization of the astrocyte and switching of V_m between the two stable states, in a down state – up state manner. If the prolonged depolarizations near V_{dr} prove experimentally plausible, such catastrophic instability would impact all aspects of the glial function, from metabolic support to membrane transport and practically all neuromodulatory roles assigned to glia.

1. Introduction

Membrane voltage control in glia - The temporal dynamics of membrane voltage (V_m) of glial cells, the non-excitable neural cells, is a difficult subject to treat due to their structure-function complexity, and the experimental limitations to precisely measure V_m by classical electrophysiological methods. The classical, more than 50 years old view of the glial membrane as *a passive potassium electrode* (Kuffler, Nicholls, & Orkand, 1966) reflected observations that K^+conductances in astrocytes accounting for the major part of ion conductivity near the resting voltage, are of Ohmic nature. It is important to note that those early observations, lacking molecular specificity, have come from studies with a rather narrow experimental focus on the glial role in ion homeostasis, i.e., in the removal of the excess extracellular K^+ following sustained neuronal firing. Intensive molecular studies in the last twenty years seriously challenged the view of purely passive electrochemical response capability of glia, upon evidence that their membrane voltage $V_m$is transiently perturbed by different electrogenic pathways through transporters and ionotropic receptors (Kettenmann & Steinhäuser, 2005), expressed with certain variations by both neurons and glia. It is now known that glial glutamate and GABA transporters, and even more intriguingly ionotropic glutamate and GABA receptors in some glia cell types (Bedner, Jabs, & Steinhäuser, 2019), do alter glial V_m, (Kettenmann, Backus, & Schachner, 1984) and therefore introduce a form of feedback control of their respective neuromodulatory functions. Observations that receptor activation leads to a transient *suspension of major potassium conductance* (Schröder, Seifert, Hüttmann, Hinterkeuser, & Steinhäuser, 2002), likely to be coupled with one of several mechanisms of Na^+intake or extrusion (Felix, Delekate, Petzold, & Rose, 2020), further requires a careful distinction of how each of those effects qualitatively and quantitatively affects the glial V_m.

Therefore, with the glial $V_m$being both, a control variable (*controller*) of different neuromodulatory loops, as well as itself being a target of neuromodulatory perturbations, the *dynamical stability of*

glial resting membrane voltage V_r in response to various perturbations is still a central question in quantitative whole-cell modeling of glia. Such a dual effect of V_m as a variable, further qualifies the glial membrane as *a sensor and transducer* of K^+ *volume transmission as a signal*, which perspective has been pushed by pioneers in the field (Ransom, 2000) but further demands explanatory biophysical models.

The typical, transient perturbations of glial V_m comes either as: (i) transient variations of local field potential which directly polarize the membrane, (ii) varying trans-junctional voltage at the gap-junction connections of heavily interconnected astrocytic cells, or (iii) as transiently altered $[K^+]_o$. Different biological control roles of glial V_m makes the stability of V_r critical for a wide range of cellular functions from glucose transport and neurotransmitter recycling, via responses to mechanical and acidic stress, to the regulation of excitation-inhibition balance in local circuits. Prospective dynamical modeling studies would try to distinguish the specific, causal responses of glial V_m to a specific form of neuromodulation, from the permanent stochastic electrochemical or other perturbations of V_m near the V_r.

Variations of V_m in a steady and perturbed glial membrane - Experimental studies of astrocytes *in* situ, the most abundant glial cell subtype, find that their V_m in nominal conditions fluctuates within a narrow range (Henneberger & Rusakov, 2012). From several millivolts, in response to nominal fluctuations of the local field, up to $10 \div 20\ mV$ more depolarized from V_r in cases of seizures, other strong synchronous discharges in the neighboring neurons and spreading depolarizations accompanied by high, transiently elevated $[K^+]_o$ (Traynelis & Dingledine, 1988), (Ballanyi, Grafe, & ten Bruggencate, 1987), or (Somjen, 2004) for review. Even though accumulated extracellular K^+depolarizes glia, it is not clear how fast, and how closely glial V_m follows the perturbed E_K when both active and passive transport mechanisms switch in, and what is in turn the sign of the driving force $\Delta V_m = V_m - E_K$ that direct the leaky currents. Typically, the reversal potential of the isolated macroscopic Kir and K2P currents is close, but slightly more positive to the Nernstian reversal potential of potassium, E_K, and closer to the cell resting voltage V_r which is typically between $-80\ mV$ to $-70\ mV$ in glial cells, *in situ*. A relevant dynamical model of V_m would thus require incorporating the *minimal*, yet detailed description of the major glial ion conductances active near V_r, over several timescales from milliseconds to minutes, under assumption it does not incorporate $[K^+]_o$ dynamics, i.e., only E_K remains a changeable parameter.

Figure 1 shows the steady-state current-voltage (I-V) recordings of the total K^+current, as well as the isolated Kir4.1 and K2P-TREK1 currents in our data, obtained under whole-cell voltage-clamp protocol in $N = 9$ freshly isolated astrocytes from mouse hippocampus, bathed in slightly elevated extracellular $[K^+]_o = 5\ mM$ (Seifert et al., 2009). In steady-state conditions under a physiological K^+ concentration gradient, the barium Ba^{2+}- sensitive *weakly rectified* Kir4.1 current (circles) dominates the total current profile (solid line). Even though much weaker in resting conditions, the K2P current (triangles) has different kinetics and electrochemical regulation, which requires to have it incorporated into any quantitation of K^+conductivity in astroglia, either experimental or theoretical.

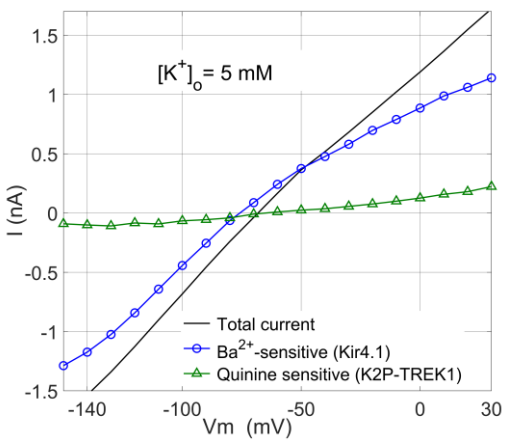

Figure 1 - Potassium current profile in isolated astrocytes – Kir4.1 current isolated as Ba^{2+}sensitive, by application of 0.1mM BaCl (blue circles/line, n=9) reverses at $V_{rev} \approx 75.35\text{mV}$, compared to the total K^+current, black solid line (data from (Seifert et al., 2009)). Of the remaining K^+conductance, K2P current (max. 0.23 nA at +30mV), was isolated as quinine-sensitive, plotted in green triangles/line. The transcript analysis of the K2P channels suggested a prevalence of K2P2.1 TREK1 isoform (Seifert et al., 2009). The sum of Kir4.1 and K2P2.1 current accounts for 82% of the total current at -120mV, and 80% at +30mV. Recordings from 9 cells, with a mean effective patch capacitance of 20 pF, have been normalized, averaged, and rescaled in the measured current range.

We described the I-V curves of the dominant K^+background currents in isolated astrocytes from mouse hippocampus (Seifert et al., 2009). The isolated K^+currents operate close to, and therefore define the resting membrane potential V_r in the proposed minimal ordinary differential equation (ODE) model of V_m dynamics. Apart of K^+ conductances, no other major conductances have been verified in astrocytes in the voltage range around V_r, assuming no osmolar stress which triggers non-negligible Cl^- transients. Co-expressed *Kir* and *K2P* channels account for the major fraction of potassium channels in almost all glial cells in the brain (Steinhäuser, 2013), cardiac fibroblast (Zuo, 2017), as well as in various cell types in renal epithelia (Hebert, 2005), (Welling, 2016). With over forty different channel isoforms in total, the co-occurrence of Kir and K2P channels in these, as well as in other tissues (Sepúlveda, 2015) is pervasive, resulting in different K^+channel mix and therefore different resulting I-V curves and kinetic properties of the currents.

Parametric analysis of the model reproducing some of the observed biological (de)regulation of those conductances suggests that astrocytic V_m could be prone to multistability in case of deregulation of the major weakly-rectified Kir4.1 current (WR-Kir). Numerical simulations of the model perturbed using realistic recordings from glia *in-situ* (Traynelis & Dingledine, 1988), illustrated the bistability of the otherwise stable resting state. Although a mix of only K^+conductances may give rise to two membrane resting states, already observed experimentally in cardiomyocytes (Zuo, 2017), and described by a simple, generic minimal 2-dimensional conductance-based model (Izhikevich, 2007), so far it has not been demonstrated in the glial membrane, or simulated numerically using a glia-specific model.

2. Model of astroglial whole-cell V_m dynamics

– Detailed electrophysiological studies of glial[1] conductances (Seifert et al., 2009) are rare, and a widely accepted minimal dynamical model of V_m in astrocytes is therefore lacking**.** Further to the experimental complexity mentioned above, depending on the model system, sometimes a specific regulation of these conductances by other physiological stimuli require quantitation.

In what follows we outline the description of experimentally measured steady-state I-V relationships of Kir4.1 and K2P-TREK1 conductances. The nonexistence of a *voltage-sensing domain* - a structure present in other *gated* K^+channels, suggests their rectification properties come from permeability regulation by physiological blocking ions, or by other Coulombic interactions on a pore level (Gonzalez et al., 2012) resulting in voltage activation. The modeling approaches to either Kir or K2P currents do not follow the Hodgkin-Huxley approach for gated channels but reflect their known biophysics and biology as open pores and the recordings of their steady-state I-V curves. The proposed models could be applied *as-are* to a different mix of those channels in different cells or tissues. In the rest of the text, for the cell-specific aspects, without loss of generality, we will refer to rodent astrocytes from the hippocampus, as our model system (Seifert et al., 2009).

2.1 Steady-state I-V model of weakly-rectified Kir current -

Since the early quantitative studies, the conductivity of Kir channels under changing $[K^+]_o$, (Hagiwara & Takahashi, 1974) indicate that Kir channels display voltage dependence on the electrochemical driving force $\Delta V_m = V_m - E_K$, rather than solely on the net membrane voltage V_m. This implies that suggested models should: (i) allow for variable $[K^+]_o$, and (ii) describe qualitative changes on different timescales, relevant not only for the millisecond V_m dynamics, but for the slower $[K^+]_o$ variations from hundreds of milliseconds to seconds and minutes, as well.

Our central modeling proposition is a detailed description of the I-V relationship of the *weakly-rectifying* potassium Kir current (WR-Kir), rather than straightforwardly assigning the Hagiwara model of a strongly inwardly-rectifying channel in egg cells (Hagiwara & Takahashi, 1974). The Hagiwara model is usually chosen under the assumption that V_m is very tightly regulated round the negative resting potential of $V_r \approx -80mV$, which is oversimplification because astrocytic V_m is exposed to perturbations that significantly depolarize the cell into a V_m range where the curves of

[1] In the rest of the text, we will interchangeably use the terms *glia, astroglia* or *astrocytes* for the population of the astrocytic cells. Where reference is made to other glial cell types, those are named specifically.

inwardly and weakly rectified Kir current markedly differ. To fill this gap requires describing quantitatively the outward conductivity of WR-Kir channels, which represent a comparable fraction to the inward component, Fig. 1 (circles).

The key modeling assumption is that the steady-state WR-Kir current, Fig. 1 (circles), could be dissected into two additive components: a) *inwardly rectifying Kir* component I_{Kir}, and b) *outwardly rectifying*, or *residual Kir component* I_{res}, so that for the total isolated Ba^{2+}-sensitive Kir4.1 current we can write:

$$I_{Kir} = I_{inw} + I_{res} \qquad (nA). \tag{1}$$

The two unidirectional fluxes result from a different manifestation of a *voltage-dependent block* of the pore by polyvalent cation which in turn result in different outward and inward permeation. Cases are known where point mutations have dominantly impacted unidirectional permeation in open pores (Wible, Tagliatela, Ficker, & Brown, 1994), (Kurata, Rapedius, Kleinman, Baukrowitz, & Nichols, 2010) We describe this using a *short-pore model* of K^+pore, formulated using a simplified description of the permeation based on one-dimensional reaction coordinate. It is generic for all K^+open pores, where the cytoplasmic domain of the channel is ignored as not critical for describing the permeation, Fig. A1, *Appendix 1*. For a detailed description of the short-pore model and further biophysical arguments on the legitimacy of modeling two separate, additive fluxes in the Kir short-pore, see *Appendix-1*.

Inwardly rectified WR-Kir flux results from a negative driving force, $\Delta V_m < 0$, where the blocking ions, Mg^{2+}or other polyvalent cations are kept within the water cavity (Fig.A1.B) of the short-pore by Coulombic forces of the negative residues of transmembrane helices (Fig. A1.A). Such ion-crowding of permeant and blocking ions (Fig. A1.B) results in an inward pseudo gating of the WR-Kir pore producing an equilibrium probability of open, inwardly conducting pore described by Boltzmann term, as originally introduced by the Hagiwara model (Hagiwara & Takahashi, 1974):

$$I_{inw} = g_{Kir-inw}(V_m - E_{Kir}) \qquad (nA) \tag{2}$$

$$g_{Kir-inw}(\Delta V_m) = \frac{A\,\bar{g}_{s-inw}\sqrt{[K]_o}}{1 + \exp\left(-z_{inw}(\Delta V_m - \Delta V_{12})/v_s\right)} \qquad (\mu S) \tag{3}$$

$$\Delta V_m = (V_m - E_{Kir}),\ \ \Delta V_{12_inw} = (V_{12-inw} - E_{Kir}) \qquad (mV),$$

where $\bar{g}_{s-inw}$ represents the maximal value of the $g_{Kir-inw}$ obtained as a slope of the linear segment in the recorded I/V curve negative of E_K, V_{12_inw} is the voltage at half-maximal conductance, z_{inw}represents the effective charge valence of permeant ions in the short-pore and $E_{Kir} = -76\,mV$ is the reversal voltage of the isolated Kir4.1 current. Figure 2A, black curve, shows a fitting sigmoid curve (3) to numerically differentiated Kir4.1 data, from Fig. 1 (blue curve, under $[K^+]_o$ = 5mM), for V_m more negative than E_{Kir}. Such numerically obtained series physically represents the conductance, whereas the values more negative to -110mV (crosses) are discarded due to slope deviation (Fig.1) originating from the voltage-dependent pore block by external Na^+(Ohmori, 1978), (Kubo, Baldwin, Jan, & Jan, 1993). The fitting gave $\bar{g}_{s-inw}\sqrt{[K]_o} = 20.6\,nS$, $V_{12_inw} = -53.5\,mV$ and $z_{inw} = 1.638$. The effective charge z_{inw}, was in accordance with published charge estimates for the voltage dependence of block by small ions, for a summary see (B. Hille, 2001). The slope factor $v_s \equiv RT/F = 25.7\,mV$, corresponding to room temperature of $T = 298.13\,K$ is kept constant throughout the text.

Outwardly rectified Kir4.1 flux results from outward pseudo gating for a more positive driving force $V_m > -60mV$ (Fig. A1.C), where outwardly directed driving force pushes partly or fully dehydrated blocking ion towards the entry of the selectivity filter (SF), see *Appendix 1.* Such electrostatic, flickering block modulates ion association to the pore and the outward permeation.

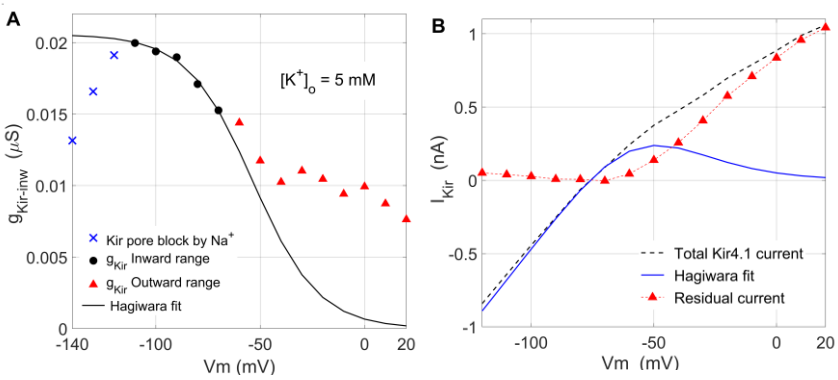

Figure 2- Separation of WR-Kir current in two unidirectional fluxes – **(A)** Fitting the conductance $g_{Kir-inw}$ by the Hagiwara model for $V_m \leq -60mV$, black line, with the crosses excluded. **(B)** The *residual outward* component, eq. (4), red triangles, obtained by subtracting the modeled inward current (blue), equation (2), from the total recorded Ba^{2+} sensitive Kir component (dashed line). Blue crosses in (A), and the small non-zero values carried over by the subtraction in (B) (red) for $V_m < -100\ mV$, result from pore block by Na^+.

To obtain numerical series for the residual, outward Kir4.1 current I_{res} (4) from the recordings, we subtracted the portion *described by the* Hagiwara model in the whole V_m range, equations (2),(3), fitted near V_r, Fig.2B, blue line, from the total Kir current, to obtain the red trace/triangles in Fig.2B.

$$I_{res} = I_{Kir} - I_{inw} \qquad (nA). \tag{4}$$

Non-constant field Goldman-Hodgkin-Katz (GHK) model of WR-Kir outward current - Meyer B. Jackson reminds us in his seminal monograph (Jackson, 2006) of several concepts always potentially applicable to an open channel when there are indications of specific pseudo-gating or macroscopic current rectification, like in potassium Kir or K2P pores. In other words, without a voltage gate as a structural determinant for gating, other features like physiological block by cytoplasmic cations may produce charge movement within the membrane or alter the Coulombic and/or structural forces defining open-pore permeability *within the single global state* of the channel.

We arrive at the proposed model of the residual current using the following assumptions:

- ***GHK formalism without the constant-field*** describes the outward conductivity, using (5) as a general form of GHK current equation before introducing the constant-field assumption (Jackson, 2006), chapter 13.13. Instead, a simple, *quadratic potential energy profile* of an elastic force $U(x) = U_{max} - w(x - x_T)^2$ introduces a parabolic energy barrier in the energy profile of an open Kir pore, Fig.3A, with the voltage drop over the pore added as linear, $V_m(x) = x\Delta V_m$. The U_{max} potential represents the peak of the *association* barrier to the permeant K^+ ion at the entry of hydrophobic SF in RT units. The barrier is centered at transition state x_T, while the positive w is the *force constant* of the elastic restoration force of Coulombic nature. For the charge in molar equivalents and the concentrations in $[mM]$, we will describe the outward current using:

$$I_{res} = zFD\frac{[K^+]_i - [K^+]_o e^{-zFV_m/RT}}{\int_a^b e^{(U(x)-zFV_m(x))/RT}dx} \qquad (nA). \tag{5}$$

  We can extend the interval (a, b) to $(-\infty, +\infty)$ because the energy profile falls sharply outside the short pore. Depending on the description of U_{max} dependence on V_m, which is a critical parameter, the location of x_T could change, resulting in an asymmetrical shape of the barrier, Fig. 3A, dashed line, compared to the symmetrical case in Fig. 3B corresponding to $\lambda_1 \neq \lambda_2$.
- ***Partial voltage-dependent pore occlusion by cytoplasmic cations activates the pore in the outward direction –*** In this model voltage-driven localization of polyvalent cytoplasmic cations in the cavity produces a partial, flickering pore occlusion, Fig. 3A, which increases the Coulombic repulsion on the permeant ion associated with the SF. Such partial blocking serves as a plausible modulatory mechanism, with the pore remaining in a single open conformation. Therefore, both, the pseudo-gating on pore-level and the macroscopic current rectification are attributed to the voltage dependence of the block. This defines a voltage-dependent probability of an activated pore with an *effective*, *equivalent charge* $z_B > 1$, reflecting the valence of the blocking ion (Mg^{2+} or positively charged polyamines), not

necessarily implicating multi-ion pore. We illustrate this blocking configuration along the reaction coordinate of the short-pore model on the sketch in Figure A1.C, as a displacement of the blocking Mg^{2+}ion from S6 (center of the cavity) towards the S5 ion coordination site (SF entrance). To formulate this modulatory blocking effect as a probability of *outward activation* in a non-gated channel, we use the Boltzmann equation in a classical way (Jackson, 2006), chapter 1.12:

$$p_{out} = {}^{1}/_{1 + e^{-z_B(V_m - V_{12-out})/v_s}}. \qquad (6)$$

Since both, the Hagiwara model of Kir pores, as well as more recent permeation studies on K2P (Schewe et al., 2016), suggested electro-chemical gating in K^+pores, with effective driving force $\Delta V_m = V_m - E_K$, applying it within Boltzmann equation cancels out the reversal potential $E_K$in (6), as it also appears in the half-activation voltage $\Delta V_{12-out} = V_{12-out} - E_K$. The slope factor v_s is the same defined within the model for inward flux.

- ***Quadratic dependence of barrier peak U_{max}* on voltage (Marcus form) -** We are adding nonlinear dependence (7) to introduce a simple form of Coulombic contribution of the voltage-dependent block in U_{max} according to (Jackson, 2006), see chapters 7.6 and 7.8:

$$U_{max}(V_m) = G_0 \left(\lambda - \frac{z_B \delta (V_m - E_K)}{4\lambda v_s G_0}\right)^2 \quad (RT\ units), \qquad (7)$$

which can describe the *saturation of outward flux* for very positive applied voltages, Fig.4, to be discussed later. Equation (7) is based on the Marcus chemical kinetics theory describing the charge transfer in chemical bonding, using reaction rate models (Marcus, 1964), which has meanwhile gained a wider acceptance in treating quasi-equilibrium changes in proteins, for review see (Matyushov, 2015). We stress that we use here qualitative features of the simplified one-dimensional reaction coordinate in the Marcus theory, *to describe* macroscopic properties, like the saturation in the voltage dependence of block in experimental measurements of whole-cell currents, rather than *to construct* a reaction rate model which is typically done for *predicting* permeation rates (Peters, 2015).

Figure 3B shows qualitatively the geometry of the Marcus energy landscape and $U_{max}(V_m)$ over the simplified, one-dimensional reaction coordinate. The peak of the barrier U_{max} at the intersection of the two parabolic wells, defines the transition state x_T, separating the left energy well where the permeant ion dwells before the outwardly directed field drives it to the SF, and the right well where the ion is associated to the pore. The critical parameter influencing U_{max} voltage dependence is the fraction of the energy profile δ, which falls under

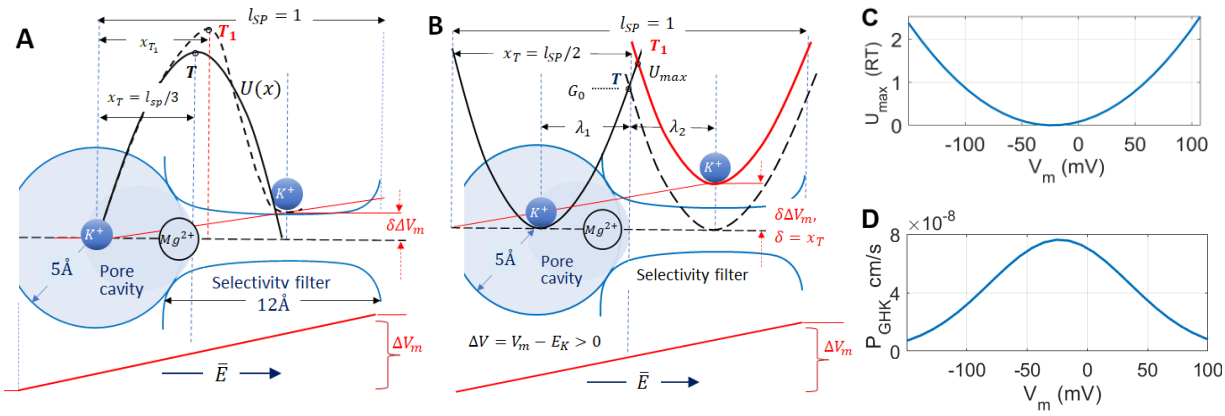

Figure 3 – Reaction coordinate in the model of WR-Kir outward permeation – **(A)** Quadratic energy barrier profile centered at the transition state x_T used in Goldman-Godgkin-Katz description of the outward flux of Kir4.1 current. Here the reaction coordinate starts at the center of the cavity, and the δV_m fraction of the voltage drops over the reaction coordinate, with a full length $l_{SP} = 1$. **(B)** Sketch of the Marcus free energy formalism defining voltage-dependence of $x_T$and the barrier height U_{max}. Voltage-dependent shift of $x_T(V_m)$ from T to $T_1$and the selection of λ_1 and λ_2 of the energy wells in (B) produce either a symmetric (solid line) or skewed barrier at the

top (dashed line) in (A). Here, compared to (A), the reaction coordinate spreads over the whole short-pore, and $x_T = 1/2$ places the peak of the barrier at the entry of SF. **(C)** and **(D)** peak behavior of U_{max} (7) and non-constant GHK permeability (9) at $V_C = -23.2\ mV$ which will produce maximal outward current I_{res}. The peak of P_{GHK} in (D) suggests that the Coulombic nature of the Mg^{2+}block facilitating the outward permeation produces a maximal P_{GHK} at V_C after what it gradually turns into full pore occlusion for more positive V_m.

the linear voltage drop, reducing it to $\delta\Delta V_m$[2]. Different positions of the transition state x_T for $\delta\Delta V_m = 0$ have been intentionally selected in Fig. 3A ($x_T = l_{SP}/3$), and 3B ($x_T = l_{SP}/2$) to illustrate the shift of x_T. Figure 3C illustrates the quadratic profile of $U_{max}(V_m)$ with the minimum attained at a critical voltage $V_C = -23.2\ mV$, at which we observe the maximal permeability $P_{GHK} = P_K = 7.63 \times 10^{-8}$ cm/s, Fig. 3D, of the same order of magnitude as the ranges in the early studies of rectification in potassium channels, see (Lu, 2004) for a review. The zero RT minimum at $U_{max}(V_C)$, Fig. 3C, should be interpreted as a zero of the *voltage-dependent potential energy profile at* x_T - where the voltage term in (7) rises the potential energy of the associated ion leveling it with G_o, the height of the entry barrier representing the image force of hydrophobic SF. Introducing nonlinear $U_{max}(V_m)$ is significant for capturing the outward WR-Kir current saturation with voltage (Meeks & Mennerick, 2007), (Edvinsson, 2011), (Gonzalez et al., 2012) which is not achieved with a constant or linearly dependent U_{max}.

Under the above assumptions, by solving the Gaussian integral in the nominator of (5) and simplifying the solution by setting a fixed position $x_T = 1/2$ (Jackson, 2006), for the outward residual component I_{res} of isolated Kir4.1 current we obtain:

$$I_{res} = p_{out}\, zFP_{GHK}\left([K^+]_i e^{\frac{zV_m}{2v_s}} - [K^+]_o e^{-\frac{zV_m}{2v_S}}\right) \qquad (nA). \qquad (8)$$

$x_T = 1/2$ places the transition state and U_{max} at the entry of the SF where the blocking ion should be localized for positive ΔV_m, which is close to 1/2 of the length of the short pore with the cavity approximately 10Å in diameter, and the SF length typically approximated to $12 \div 15$Å, depending on the structure-function assumptions. The simplification removes $x_T(\Delta V_m)$ shift which, for illustration, for $\Delta V_m = v_s$, $l = 1/4$, with $z_B = 1.6$ and $G_o = 6.6\ RT$ obtained by fitting (8) to the data (4), shifts x_T from 0.5 to 0.56.

Having departed from the classical Nernst-Planck description of the open pore to an alternative form of GHK equation for the macroscopic I_{res} in (5) and (8), extended with modulation of permeability by voltage-dependent block, we implicitly define voltage-dependent permeability (9) (Jackson, 2006).

$$P_{GHK}(V_m) = \sqrt{\frac{w}{\pi RT}}\, D\, e^{-\frac{U_{max}(V_m)}{RT}} = P_K e^{-\frac{U_{\max}(V_m)}{RT}} \qquad (cm/s). \qquad (9)$$

Here w is the same force factor from the harmonic potential $U(x)$, and D is the classical, constant diffusion coefficient, both absorbed within the constant, voltage-independent K^+permeability P_K multiplied by a factor of Arrhenius activation form with voltage-dependent barrier $U_{max}(V_m)$. For other studies where explicit, nonlinear dependence of GHK permeability has been used, mostly in neuronal calcium channels, see (Borg-Graham, 1999).

[2] δ represents a fractional, dimensionless, "electrical" length of the pore or permeation coordinate $0 \geq \delta \geq l_{SP} \equiv 1$.

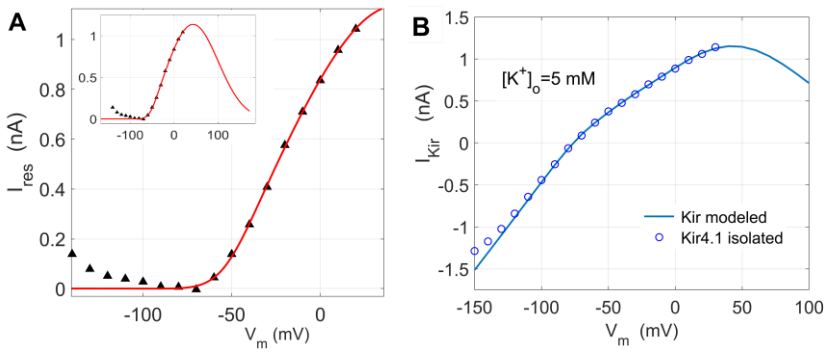

Figure 4 – Fitting the I_{res}model to data – (**A**) Numerical fit of I_{res} model (10), red curve, to the data series obtained using (4), black triangles. The inset shows the same curve extended to more positive voltages, displaying a peak behavior outside the typical V_m range. (**B**) The total modeled Kir current I_{Kir}, (10), solid line, apart from the close match with the total isolated Kir4.1 current, (circles), displays the peak behavior with V_m.

For the final form of the Kir current model to fit the isolated Kir4.1 current recordings, we get:

$$I_{Kir} = I_{inw} + I_{res} \qquad (nA)$$

$$I_{inw} = g_{Kir}(V_m - E_K) = \frac{A\,\bar{g}_{s-inw}\sqrt{[K^+]_o}}{1 + e^{-z_{inw}(V_m - V_{12})/v_s}}(V_m - E_K) \quad (nA) \qquad (10)$$

$$I_{res} = p_{out} z F P_K e^{-U_{max}/RT}\left([K^+]_i e^{\left(\frac{zV_m}{2v_s}\right)} - [K^+]_o e^{\frac{zV_m}{2v_s}}\right) \quad (nA).$$

Fitting I_{res} model (10) with U_{max} given by (7) to the residual outward current data obtained by (4), using nonlinear least-squares error, gives the I-V graph in Figure 4A. The peak behavior in (7) produces the declining slope in the rise of I_{res} and a peak behavior in a wider positive, non-physiological V_m range for glia, Fig.4B, as already reported in a study of a whole rodent hippocampus (Meeks & Mennerick, 2007), with the curve shifted to more negative voltages.

All the parameter values, fixed and obtained by fitting are listed in Table 1. The table values of I_{res} fitting parameters: $P_K, V_{12-out}, G_0, z_B$, and z, to be later used in the parameter analysis of the model, were obtained as averages of ten curve fitting attempts with one of them varied within $\pm 10\%$ of the initial value in each run while the other four were recalculated by the NLSQ curve fitting. The blocking ion charge valence was bounded within $1.5 \leq z_B \leq 2.0$. The goodness of fit $R^2 \geq 0.98$ was achieved in all attempts.

2.2 Steady-state I-V model of K2P-TREK1 current – Studies isolating the weaker astrocytic currents after isolating Kir currents are rare, due to experimental issues with leaky astrocytic membrane, and therefore K2P currents are rarely quantified (Seifert et al., 2009), (Zhou M., 2009). Figure 5A shows pharmacologically isolated K2P current, using *quinine*, at $[K^+]_o = 5\ mM$ (black circles), as well as at drastically elevated external potassium at $[K^+]_o = 50\ mM$ (blue dots) in our data from (Seifert et al., 2009). Both I-V recordings were fitted (solid lines) with the standard GHK current equation (Chen, 2014), even though the permeation studies suggest multi-ion occupancy of the pore and some form of pseudo gating (Schewe et al., 2016). Adding a small Na^+permeability (Chen, 2014), $P_{Na}/P_K = 0.06$, within nominally non-conductive range (below $-50\ mV$) improves the fit at $5\ mM$, solid purple line. That effect of Na^+on passive K^+ conductivity in glia is known (Ransom & Goldring, 1973), but we didn't use the correction within the numerical simulations due to a lack of recordings to verify P_{Na}/P_K dependence itself on $[K^+]_o$ for notably elevated levels above 5 mM.

The K2P currents in this study (Seifert et al., 2009) originate primarily from the K2P-TREK1 sub-population of K2P channels. TREK1 channels are polymodal transducers of different cellular stimuli (Honore, 2007), (Enyedi & Czirjak, 2010), like mechanical pressure or pH shifts that transduce into changes of V_m, so that any distinction between steady-state and activated state of these and most of others K2P channels requires careful consideration, both experimental and biophysical. Working with steady-state recordings from astrocytes isolated in a bath assures that obtained I-V curves represent cells in steady conditions, non-transducing an osmolar stress or pH variations, which is implicitly assumed in a baseline model.

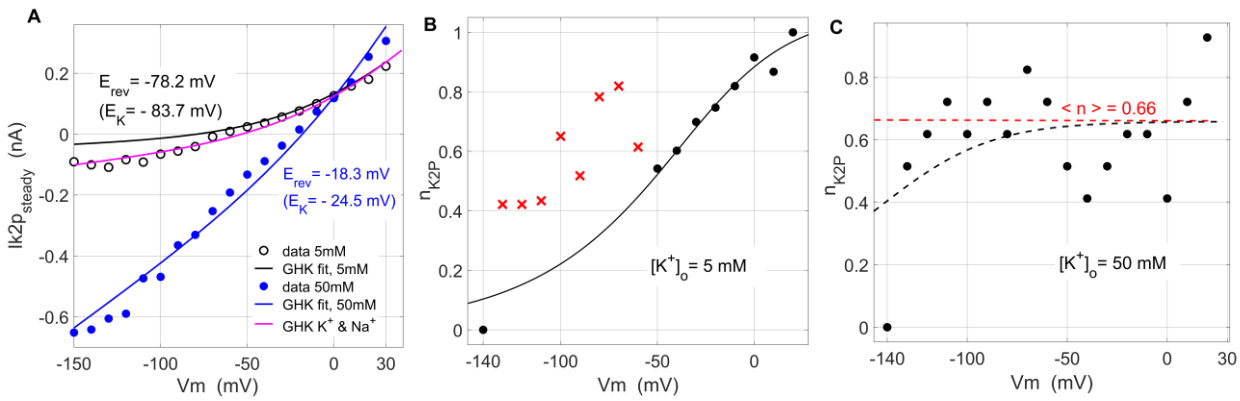

Figure 5 - Steady-state I-V relationships and activation kinetics of K2P-TREK1 currents in astrocytes – (A) Steady-state I-V characteristics of K2P-TREK1 currents fitted with the Goldman-Hodgkin-Katz current equation, for $[K^+]_o$ = 5mM (black circles/line) and 50mM (blue circles/line). The purple curve shows the fit corrected with a small Na^+permeability being added ($P_{Na+}/P_{K+} = 0.06$, see text). **(B)** and **(C)** Approximation of the activation kinetics $n_{K2P}(V)$ of K2P current for $[K^+]_o$ = 5mM and 50mM respectively, obtained as $(g_{slope}\ /\ \bar{g}_{max}\ )$^$(1/k)$, $k = 2$, see text. At 5mM **(B)** the n_{K2P} activation estimates for V_m positive to $-50mV$ (black circles) were fitted with Boltzmann first-order activation kinetics, ignoring more negative V_m values where very small currents produced erratic estimates of g_{slope}, approximated by numerical differentiation (red crosses). **(C)** The loss of voltage-dependent activation n_{K2P} (as seen in B) when switching to $[K^+]_o = 50\ mM$ was modeled as a gradual $[K^+]_o$- *dependent shift* of the n_{K2P} curve (see eq. 12b) to the left practically removing the sigmoidal voltage dependence and reducing n_{K2P} to fluctuations around a mean, constant activation $\langle n_{K2P} \rangle = 0.66$, for voltages in the activated range for K2P current.

Apart from the outward voltage activation (verified also in a symmetrical K^+concentrations), K2P channels show also *electrochemical activation* component coming from multi-ion occupancy of the pore by the permeant K^+ions (Schewe et al., 2016). The following two dynamical properties in voltage-dependent activation of K2P-TREK1 current are critical for demonstrating nontrivial behavior in the dynamic model of V_m:

- **Activation kinetics** - At both concentrations, the whole-cell currents showed activation kinetics with $\tau_{K2P} \approx 3\ ms$, constant over the whole V_m range. While at $5\ mM$, above $-50\ mV$ we could fit a Boltzmann sigmoidal, voltage-dependent activation, Fig. 5B black dots, at drastically elevated, $[K^+]_o = 50mM$ there is no visible voltage dependence, Fig. 5C, described with a constant average activation of $\langle n_{K2P} \rangle = 0.66$.
- **Gating mode change** – At elevated external K^+, Fig. 5A, the dominating *electrochemical activation* (Schewe et al., 2016) is changing the I-V curve, resembling more that of the leaky K2P-TWIK channels with almost linear dependence, satisfying the GHK current equation and reversing close to the Nernst potential.

Along with these observations we model the astrocytic K2P-TREK1 currents using the GHK current model (Chen, 2014), extended with *electrochemically dependent* activation n_{K2P} – coupling the voltage-dependent activation and electrochemical driving force into a mechanism named *ion-flux gating* (Schewe et al., 2016):

$$I_{K2P} = n_{K2P}^k\, I_{K2p-GHK}$$
$$= n_{K2P}^k\, P_{K2P} \frac{F^2 z_{K2P}^2}{RT} (V_m - V_{ofs}) \frac{([K^+]_i - [K^+]_o \exp(-z_{K2P}(V_m - V_{ofs})/v_s))}{(1 - \exp(-z_{K2P}(V_m - V_{ofs})/v_s))}\ (nA). \qquad (11)$$

Allowing for variations of K^+concentrations we cannot keep the intrinsic permeability P_{K2P} constant (Eisenman, 1983), contrary to the classical assumptions based on the solubility-diffusion theory (B. Hille, 2001), (Johnston, 1995). To add a simple $[K^+]_o$ dependence in P_{K2P} we interpolated the fitted values for P_{K2P} at 5mM and 50mM with an increasing and slowly saturating K^+dependence (12a). The GHK fit at 5mM suggested $P_{K2P}^b = 1.24 \text{ x } 10^{-8} cm/s$ for the baseline permeability, within the order of magnitude with those reported in the early studies of electro-diffusion in K^+channels, (Hodgkin & Horowicz, 1959). Fitting of the sigmoid in Fig.5B to $(g_{slope}\ /\ \bar{g}_{max}\ )^{(1/k)}$ graph obtained

by differentiation for both concentrations was done with $k = 2$, following the average ion occupancy of the SF with $2.2\ e_0$ elementary charge units across different K2P channel subtypes, estimated in (Schewe et al., 2016). Small voltage offset V_{ofs} not exceeding $5\ mV$ was needed to stabilize numerically the nonlinear LSQ fitting of (11). A same $z_{K2P} = 1$ value was used in both K^+concentrations.

$[K^+]_o^b$ the nominal, baseline external concentration in (12a) was kept at $2.5\ mM$. To correct the n_{K2P} activation for variable concentrations two interventions are needed: (i) decreasing trend of the maximal activation with $[K^+]_o$ (12b), where the $[K^+]_o/[K^+]_i$ term successfully captures the trend, and (ii) shifting the V_{12-K2P} (12c) and the whole n_{K2P} sigmoid to the left (into non-physiological hyperpolarized range) so that the plateau of $\langle n_{K2P} \rangle = 0.66$ covers the most of physiological V_m range - practically removing voltage-dependent activation, Fig. 5C. More recordings on different $[K^+]_o$ are needed to verify whether the suggested corrections in (12b) and (12c) have more general biophysical value. The shift of Nernstian nature in (12c) required a scaling factor $S = 1.7$ to get the plateau-like in Fig. 5C. Similar proportionality of V_{12} shift was observed in human K2P-TREK1 channels expressed in *Xenopus* oocytes (Schewe et al., 2016).

$$P_{K2P} = P_{K2P}^b(1 + 0.85\log_{10}([K^+]_o/[K^+]_o^b)) \quad (cm/s), \tag{12a}$$

$$n_{K2P}(V, [K^+]_o) = \frac{1 - [K^+]_o/[K^+]_i}{(1 + \exp(-z_{K2P}F(V - V_{12_K2P})/RT))}, \tag{12b}$$

$$V_{12-K2P}([K^+]_o) = V_{12-K2p}^0 - S\ln([K^+]_o/[K^+]_o^b)\frac{RT}{z_{K2P}F} \quad (mV). \tag{12c}$$

Equation (11) fuses (i) the modified voltage-dependent and $[K^+]_o$- corrected n_{K2P} activation (12b) describing an arbitrary K2P channel population, and (ii) the nonlinear Goldman-Hodgkin-Katz electro-diffusion describing the macroscopic steady-state current of the whole, voltage-clamped cell. The GHK current model extended with activation kinetics has already been used in descriptions of neuronal voltage-gated calcium channels (Destexhe, 2000).

2.3 Full dynamical model of glial V_m – The dynamics of the astrocytic membrane voltage $V_m$is described by the differential equations (13), where to Kirchhoff's current law a single kinetics equation has been coupled, that of K2P channel activation n.

$$\begin{aligned} C_m\, dV_m/dt &= -(I_{Kir} + I_{K2P} + I_{leak}) + I_{ext} \quad (nA) \\ dn/dt &= (n_{K2P}(V_m) - n)/\tau_{K2P}. \end{aligned} \tag{13}$$

An unspecific, potassium Ohmic leak current is added as $I_{leak} = g_{leak}(V_m - E_K)$ with the conductance not exceeding 15% of the chord conductance of total glial K^+current in the I-V plot, proportional to the current that remains after isolating Kir and K2P currents, Fig 1.

The external inputs, to resemble external currents to an astrocyte *in situ*, are represented as:

$$\begin{aligned} I_{ext} &= I_{gjc} + I_{lfp} \quad (nA) \\ I_{gjc} &\sim \sum_i g_c^i(V_m^i - V_m) = const. \quad (nA) \qquad i = 1,..N_{neighbors} \\ I_{lfp}(t) &= g_{lfp}V_{lfp}(t) \quad (nA), \end{aligned} \tag{14}$$

where I_{gjc} brings in the contribution from all neighboring astrocytes connected via Ohmic gap junction connections (GJCs) and will be varied as a parameter, while $I_{lfp}(t)$ represent the transient, time-dependent variable depolarization of the membrane coming from the changing local field

potential immediate to the astrocytic membrane, resulting from major prolonged neuronal spiking episodes.

Parameter	Units	Description	Value, default	Comment
T	K	Temperature	298	Room temperature, 25˚C in (Seifert et al., 2009)
F	$C/mole$	Faraday constant	96485	
R	$J/mole \cdot K$	Universal gas constant	8.314	
v_k	mV	Slope factor, RT/F	25.7	at $T = 298°K$, constant in all models and simulations
$[K^+]_o^{nom}$	mM	Baseline $[K^+]_o$in extracellular space	2.5 – 5	5mM used in I-V fitting, varied within param. analysis
$[K^+]_i$	mM	Astrocytic $[K^+]_i$	130	
C_m	pF	Astrocytic membrane capacitance	20	Mean effective capacitance of the patch, whole-cell
$\bar{g}_{s-inw}$	μS	Max. Kir inward slope conductance	0.00917	Hagiwara model of Kir current, Eq. (3)
A	$1/mM^{1/2}$	Dim. constant, correcting for $\sqrt{[K^+]_o}$	1	Dimensionality correction
V_{12-nom}	mV	Half-activation voltage V_{12} at $[K^+]_o^{nom}$	-53.5	Hagiwara model of Kir current, Eq. (3)
z_{inw}		Effective charge valence, I_{Kir}	1.638	Hagiwara model of Kir current, Eq. (3)
z		Unitary valence of permeant K^+ions	1.0	
$E_{rev-Kir}$	mV	Rev. voltage of isolated Kir4.1 current	-76	Exp. measured rev. Voltage, constant
P_K	cm/s	Constant permeability of K^+in pores	7.63e-08	K^+permeability in classical Nernst-Planck formalism
$V_{12-out0}$	mV	Half-activation voltage of I_{res}	-51.4	Boltzmann term in p_0 , Eq. (6)
z_B		Effective charge valence of the blocker	1.6	Mg^{2+}or polyamine blocking ion
G_0	RT units	Voltage-independent entry barrier	6.6	Barrier height at transition state, Marcus term, Eq. (7)
l_{SP}		Normalized, unitary length of the pore	1	Short pore model, Fig. A1
x_T		Fractional distance of transition state	1/2	Position relative to the beginning of the pore
λ		Half-width of the energy wells	1/4	Marcus term, Eq. (7) and Fig. 3
δ		Fractional, electrical length of the pore	1/2	Fraction of l_{SP} over which $V_m$drops, Marcus term, Eq. (7)
V_{12-K2p}^0	mV	Half activation voltage V_{12} at $[K^+]_o^{nom}$	-20.5	I_{K2P} model, n_{K2P} activation, Eq. (12c)
k		k-th power in K2P activation kinetics	2	Hodgkin-Huxley formalism, Eq. (11)
S		Scaling parameter in n_{K2P} activation	1.7	Adjusts the shift of n_{K2P} with $[K^+]_o$, Eq. (12c)
z_{K2P}		Charge valence for K2P pores, fixed	1.0	I_{K2P} model, Eq. (11) and n_{K2P} activation Eq. (12b)
τ_{K2P}	ms	Activation time of K2P-TREK pore	3.0	From exp. data (Seifert et al., 2009), Eq. (12b)
P_{K2P}^b	cm/s	K2P channel permeability, basal	1.24e-08	I_{K2P} model, GHK description, Eq. (12a),
g_{leak}	μS	Glial leak conductance, Ohmic	0.001-0.002	Non-specific leak, glial voltage dynamics, Eq. (13)
I_{ext}	nA	External current to the astrocyte	0.2 - 0.4	Glial voltage dynamics, Eq. (13)
g_{lfp}	μS	Transfer conductance in resp. to V_{lfp}	0.01-0.016	Adjusted to the I_{ext} ranges in bifurcation analysis

Table 1 – Parameter values used in the fitting of current models, parametric analysis, and simulations of the full system (13).

It has been already shown that equation (13) represents a minimal model where only K^+ conductances, without any Na^+or Ca^{2+}contributions could produce more complex dynamical behavior of V_m than a stable fixed point V_r (Izhikevich, 2007).

Table 1. contains all the parameter values and/or value ranges used in the dynamical analysis of the model and the numerical simulations of transiently perturbed behavior.

3. Results

3.1 Parametric analysis of the V_m dynamics

When translating the nature and the intensity of the perturbations in real cells in different experimental preparations into changes of model parameters, we will refer to (a) *static*[3] *alterations* of the astrocytic K^+ conductances to changes manifesting in the steady-state I-V relationships, and to (b) *dynamical perturbations* of V_m in (13) for response to transient changes in the local field potential, depolarizations through the gap-junctions, or response to transient shifts of $[K^+]_o$.

Of not many studies differentially isolating glial currents (mostly focusing on Kir), we looked for those where the changes *would* alter the monotonic I-V dependence of the total astrocytic current, Fig. 1. For a summary of changes, and the source references see Table 2 in *Appendix 2*. Sole focus on Kir currents with K2P current not being isolated has prevented those studies to report the impact of altered Kir current on the I-V curve of total current. The alterations of Kir currents summarized in Table 2 suggest that the model should consider asymmetrical changes of Kir conductivity in different V_m ranges, either as a hallmark of a pathology or different functional channel expressions like in the case of heteromeric Kir4.1/Kir5.1 channels. Biophysical specificity of the Kir4.1/Kir5.1 channel is that it turns weakly rectifying Kir4.1 into a strong inward rectifier (Marmolejo-Murillo et al., 2021), numerically equivalent to almost fully attenuating the outward I_{res} current.

Figure 6A illustrates the trend of change in the steady-state I-V curve of the total K^+ current in different scenarios of Kir deregulation. A typical effect is a loss of monotonicity positive to $+60mV$, where both Kir4.1 and K2P currents coexist producing a non-monotonous N-shaped I-V curve. In Figure 6 we sketched this effect by different attenuations of Kir inward and/or outward component in our model, based on the observations in different disease models, Table 2. Included also, the yellow curve, is the combined effect of loss of outward Kir conductance in parallel with drastically increased $[K^+]_o$ like in cases of seizures and spreading depolarizations. To produce the effects in Fig. 6A we were (a) decreasing $\bar{g}_{s-inw}$ for the inward range of WR-Kir current in Hagiwara model (3), and (b) doing the same using a multiplier in the GHK model (8) for the outward range, due to a complex form of the conductance in I_{res} model. The K2P current was kept in the nominal range and shape.

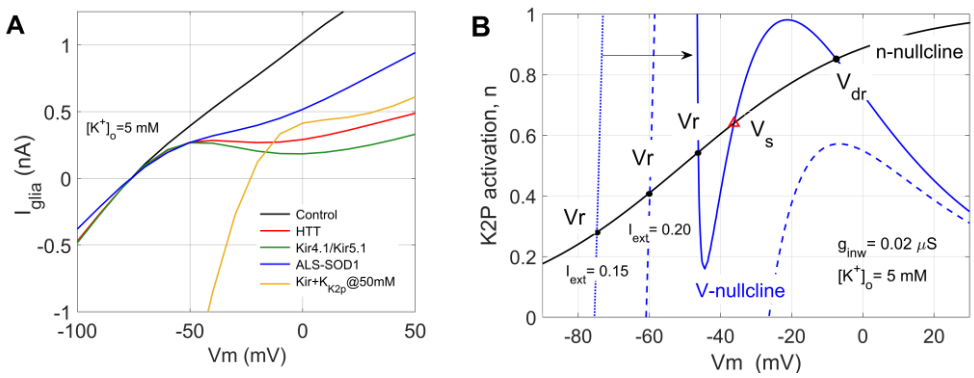

Figure 6 – Loss of monotonic I-V curve via alterations of Kir4.1 currents in disease models. (**A**) Alterations in Kir conductivity without changes in K2P conductance produce non-monotonic I-V curves. The yellow curve illustrates the parallel effect of a drastic increase in external K^+, while all others are obtained by amplifying or attenuating the modeled Kir currents at $[K^+]_o = 5mM$ based on the nature of deregulation in Table 2. The labels in the legend relates each curve to the corresponding study in Table 2. (**B**) Example of nullcline analysis in (V_m, n) plane. Increasing the constant I_{ext} changes (into an N-shape) and shifts the V-nullcline introducing a saddle fixed point V_S (red triangle), and markedly more positive stable node or focus V_{dr} via the fold bifurcation. The dotted, dashed, and the full blue line show the changing shape of the V-nullcline with I_{iext}.

[3] Even though the channel expressions change in time, those happen on time scales of minutes, hours or longer, which warrants keeping the corresponding parameters constant on timescales of milliseconds or seconds.

Since the typical dynamic perturbations, same as with neurons transiently depolarize the glial membrane by I_{gjc} or $I_{lfp}(t)$ currents, the principal bifurcation parameter was a constant in time I_{ext}. As a second bifurcation parameter, we varied $\bar{g}_{s-inw}$ and $[K^+]_o$ with attenuation of I_{res} as a static perturbation of the model, so that all scenarios of impact on Kir conductivity could be implemented.

In the 2-dimensional system (13), using nullclines let us detect the trends of change in the phase portrait. As expected and previously illustrated in models of neurons very similar to (13) (Izhikevich, 2007), chapter 5, in addition to the single equilibrium state V_r - a stable node for V_m slightly more positive to E_K, the N-shaped I-V curve introduces multiple steady states via the fold bifurcation, as we vary I_{ext}, Fig. 6B. The fold bifurcation is generically present in 2-d models like (13) with N-shaped nonlinearity in the voltage[4] equation and robustly observed within wide parameter ranges. We keep referring in the rest of the text to the nominal stable, resting state as V_r, and to the more depolarized, again stable steady-state introduced by the fold bifurcation as V_{dr}.

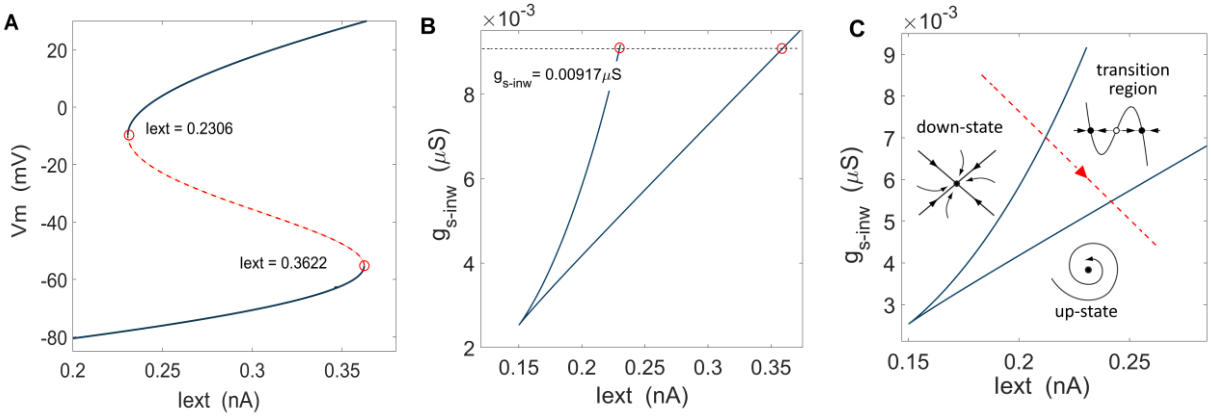

Figure 7 – **Fold bifurcations in (V_m, n_{K2P}) dynamics** are generic when the perturbed model displays an N-shaped I-V characteristic. (**A**) Fold bifurcation diagram of (13) for $g_{s-inw} = 0.00917\ \mu S$, with I_{res}= 0. (**B**) A cusp curve in (I_{ext}, g_{s-inw}) plane obtained by running 2-parameter continuation from the fold point at $I_{ext} = 0.2306$ in (A). The coordinates of the corresponding stable steady states are $(V_r = -77.86\ mV, n_{K2P} = 0.0964)$, and of the saddle-node close to $(V_{dr} = -9.734\ mV, n_{K2P} = 0.6)$, with g_{s-inw} kept at the same value as in (A). (**C**) The red dashed line shows a typical path through the parameter plane corresponding to a membrane with deregulated Kir conductance perturbed by a net depolarizing current I_{ext}. The region bounded by the cusp curve separates the two *monostable* parameter domains, the down-state domain, corresponding to the true nominal resting state V_r (of node type), and that of the up-state, corresponding to a *single* depolarized steady state V_{dr}, of focus/spiral type. For parameter values inside the transition region, within the cusp, the model displays two stable nodes separated by an unstable saddle point.

Figure 7A and 7B show the fold and cusp bifurcation diagrams for changing I_{ext} and g_{s-inw}, with the outward I_{res} attenuated. All continuations were done using the *AUTO* package (Doedel et al., 1997) as implemented within *XPPAUT* (Ermentrout, 2002). Examples in Fig.7A and 7B were computed with $I_{res} = 0$, though qualitatively the same behavior is present with I_{res} between zero and 15% of its intensity. All other model parameters were kept at the values given in Table 1, used in the fitting of steady-state I-V characteristics, with $[K^+]_o = 2.5\ mM$ and the glial leak $g_{leak} = 0.0013\ \mu S$. At $I_{ext} = 0.2306\ nA$, in Fig. 7A the bifurcation introduces a saddle-node at $V_{dr} = -9.734\ mV$, notably depolarized to the nominal $V_r = -77.86\ mV$, which further splits into a saddle and stable node at V_{dr} as I_{ext}further increases. The cusp curve Fig. 7B fusing fold bifurcation behavior of two parameters divides the (I_{ext}, g_{s-inw}) plane in three regions: (I) the *down-state* represented by V_r, (II) the *up-state* represented by the depolarized resting voltage V_{dr}, and (III) the bistability region where V_m transits towards either of the equilibria, qualifying the model for switching behavior. We borrowed these terms from models of neuronal excitability since both neurons and glia share the same feature - the true resting state near E_k which gets excited by a shift of V_m to more positive values. Equations (13) represent the first minimal mathematical model of the glial membrane near V_r, based on whole-cell

[4] We refer to the first ODE in (13) as *voltage equation* because it describes the dV_m/dt derivative, even though as a physical law it is the Kirchhoff's current equation.

recordings, suggesting the existence of a stable, depolarized up-state in glial V_m dynamics, within a wide range of parameters.

The biological relevance of downregulating or abolishing the WR-Kir outward I_{res} current as a parametric perturbation is directly suggested by (1) electrophysiological data in several disease models we listed (Tong, 2014), (Bataveljić, 2012), as well as (2) by the specific properties of heteromeric Kir4.1/Kir5.1 channel populations (Hibino et al., 2010), (Marmolejo-Murillo et al., 2021). The later accounts for a nonnegligible fraction of Kir4.1/Kir5.1 channels in astrocytes in different brain regions (Hibino, Fujita, Iwai, Yamada, & Kurachi, 2004), (Soe, Andreasen, & Klaerke, 2009), (Seifert et al., 2009). The extent of deregulation of the *inward conductance of the Kir4.1 alone* – a decreased slope in the I-V curve negative to V_r, is not detrimental for the observed qualitative changes since it doesn't produce by itself the N-shaped I-V curve.

The dashed line in Fig. 7C represents a typical *perturbation line* of (13) combining (i) permanent deregulation of outward conductance of WR-Kir, with (ii) changing inward WR-Kir conductance in experimental conditions where an astrocyte is (iii) subjected to depolarizing current input I_{ext}.

Slow depolarizations induced by K^+accumulation in extracellular space (ECS), and subsequently the positive shift of E_K and V_r suggest that either as a parameter, a transient perturbation, or a slow variable in an extended 3-dimensional model, $[K^+]_o$ could be inducing instability of V_r. Since an extension of the system (13) by incorporating $[K^+]_o$ dynamics in R^3or higher (Barreto & Cressman, 2011) is beyond this study, we verified that fold and cusp are robust in $(I_{ext},\ [K^+]_o)$ parameter domains as well, with I_{ext} in the same range as above, and $[K^+]_o$ modestly raised compared to the nominal $2.5\ mM$, Fig. 8.

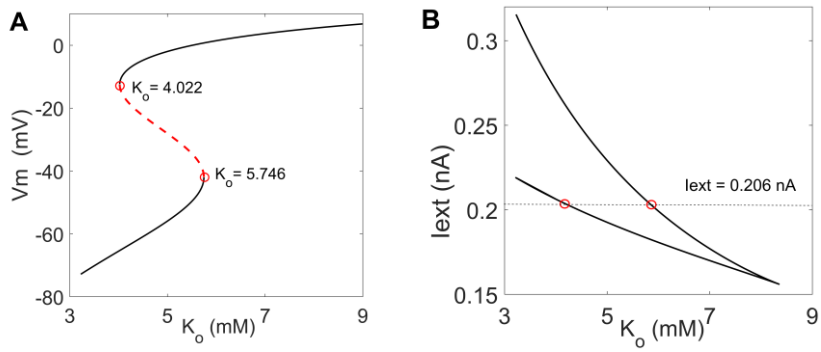

Figure 8 - Fold bifurcations under variable $[K^+]_o$ with abolished I_{res} (**A**) Fold bifurcation (13) for variable $[K^+]_o$, keeping $g_{s-inw} = 0.00951\ \mu S$. (**B**) A cusp curve in $(I_{ext}, [K^+]_o)$ plane obtained by running 2-parameter continuation from the fold point at $[K^+]_o = 4.022$ in (A). The actual continuations were computed using E_K due to better numerical convergence. $[K^+]_o = 4.022\ mM$ corresponds to $E_K = -89.32\ mV$, for $[K^+]_i = 130\ mM$

Large separation of time scales between V_m responses and $[K^+]_o$ transients, from milliseconds to second and minutes, warrants analyzing the basic $[K^+]_o$ impacts on V_r stability treating it as a parameter in the simple 2-dimensional system (13).

Quantitative studies summarizing the properties of macroscopic currents through the glial Kir4.1 (Seifert G., 2018) and K2P-TREK channels (Schewe et al., 2016), (Chen, 2014) suggest that apart from K2P activation there is no other channel kinetics critical to extend (13) with additional dynamical variable. Whole-cell Kir4.1 currents were showing rise times of less than $2\ ms$ and negligible difference between the peak and steady current levels, in the mid-range voltages V_m where the interaction of different currents is dynamically interesting. As a result, there is no candidate for a *resonant variable* in the 2-D model (13) (Izhikevich, 2007), (Izhikevich, 2004) which would induce a cyclic behavior in the minimal, 2-dimensional autonomous system (13).

3.2 Numerical simulations of the bistability and switching

For demonstrating the switching capability we perturbed the model (13) using time series from recordings of glial depolarization during *electrographic seizures* induced by transient elevation of $[K^+]_o$ (Traynelis & Dingledine, 1988). The glial V_m was recorded using two-electrode *in-situ* protocol on glial membrane in rodent hippocampal slices.

Figure 9, (upper trace) shows a sample of glial depolarization ΔV_{lfp} referenced to an LFP of a near electrode, in response to neuronal seizure, Fig. 11A, in (Traynelis & Dingledine, 1988), digitized from a printed image using the *Graph Grabber* tool (Benbow, 2020). Such *voltage generator signal*

features: (i) a fast depolarizing, tonic transient of $\Delta V_m \approx 20mV$ within initial ten seconds, followed by (ii) pseudo-periodic clonic episodes lasting in total for nearly 60 seconds. To use the ΔV_{lfp} recording as a perturbing signal in our model (13) we need somewhat realistic time course of the corresponding $\Delta E_K(t)$ shift, for which purpose we used ΔV_{lfp-dc} averaged signal of 135 seizure events, the lower curve in Figure 9, see Fig. 10A, in (Traynelis & Dingledine, 1988), where as well the measurement electrode on glia has been referenced to the LFP immediately adjacent to the glial cell body, so that for I_{ext} in (14) we get:

$$\begin{aligned} I_{ext}(t) &= I_{gjc} + I_{lfp}(t) = I_{gjc} + g_{lfp}\Delta V_{lfp}(t) \quad (nA) \\ E_K(t) &= E_K + \Delta E_K(t) \approx E_K + \Delta V_{lfp-dc}(t) \quad (mV) \\ \Delta V_{lfp-dc} &= \langle \Delta V_{lfp} \rangle_i - \langle \Delta V_{lfp} \rangle_o \quad (mV). \end{aligned} \tag{15}$$

Perturbation signals as in (15) mimic a transient depolarization event of a hippocampal glial cell *in situ*, depolarized by a positive, outward current resulting from sustained seizure-like discharges invading the surrounding neurons in a larger region, slowly and transiently elevating, and restoring the nominal $[K^+]_o$ during 72.6 seconds. Therefore, we do not simulate bath application of a constant elevated $[K^+]_o$ from (Traynelis & Dingledine, 1988), where apart from some brief, transient local variations of $[K^+]_o$ it has been kept constant, but try to simulate more realistic transient depolarization which in reality comes with transiently altered local $\Delta E_K(t)$.

We find ΔV_{lfp-dc} to be a good example of $\Delta E_K(t)$ assuming it represents an average of LFP events (a) already subjected to low-pass filtering of the ECS (Bedard, Kroger, & Destexhe, 2006), and (b) of comparable shape in the initial steady depolarization phase, time-aligned at the onset. Its maximal amplitude of $12.8mV$ is close to the Nernstian $\Delta E_K = 13.7\ mV$, corresponding to a shift of $[K^+]_o$ from the nominal 5 mM in our data (the nominal I-V relations in the model), to 8.5 mM bath concentration robustly producing the seizures (Traynelis & Dingledine, 1988). The slower rise time in the initial 10 seconds, as well as the steady decay of the averaged $\Delta V_{lfp-dc}(t)$ reflect the action of the Na-K pump and other restorative mechanisms of ion homeostasis. Such $\Delta E_K(t)$ is therefore a safe choice for low to moderate $[K^+]_o$ increases on the timescale of seconds, even a more conservative one, producing slightly less depolarized E_K shifts if we start from a baseline of $2.5\ mM$ of external K^+. Unspecific conductance $g_{lfp}$was introduced to convert the transient voltage perturbation $\Delta V_{lfp}(t)$ into current perturbation signal in (15). Indicative value range was set between $0.01 \div 0.0155\ \mu S$ to keep the total $I_{ext}(t)$ in simulations within the range of the fold bifurcation diagram, Fig. 7A, matching the dynamic range of the clonic discharges in ΔV_{lfp} of $5 \div 10\ mV$, from $t = 10\ s$ onwards, Fig. 8.

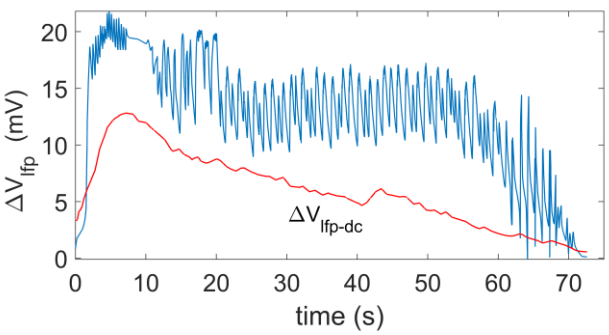

Figure 9 – Transient glial depolarization signals – Depolarization transient ΔV_{lfp} from resting (upper trace) measured on glial soma *in situ*, in response to an electrographic seizure initiated by increased $[K^+]_o$ to 8.5mM, in a rat hippocampal slice. A two-electrode protocol was used with a reference electrode in the bath. ΔV_{lfp-dc} (lower trace) is an average of 135 depolarizing episodes, recorded from 5 cells, used to approximate the shift of the Nernstian potential $\Delta E_K(t)$ due to K^+ accumulation.

A simulated example of switching behavior in response to the above perturbing transients is illustrated in Figure 10. Dotted lines are V_m responses from ten solutions of (13) perturbed with $I_{ext}(t)$ with $0.01 \leq g_{lfp} \leq 0.0155$, $I_{gjc} = 0.2$, at $[K^+]_o = 2.5\ mM$ and $g_{s-inw} = 0.00917\ \mu S$, with outward WR-Kir current reduced to 10% of its amplitude. Qualitatively the glial V_m is quenching the clonic discharges to a few millivolt variations, but around two different voltage baselines corresponding to the down-state or the up-state, depending on g_{lfp} value. For $0.0137 \leq g_{lfp} \leq 0.014\ \mu S$, after the tonic transient, the responses do not follow the shape of the perturbation but

mark some form of boundary or a *separatrix response* or *no-man-land* of V_m. Beneath and above that g_{lfp} range the glial membrane responded with an expected waveform, either close to the down-state V_r, or with a depolarized transient around the up-state V_{dr}. The bold black lines show an average of ten runs with randomized (g_{lfp}, g_{s-inw}) values within 10% variation, for each of the three qualitatively distinct responses. No particular sensitivity to either of the parameters was observed indicating a hidden peculiar singular behavior, in dynamical terms.

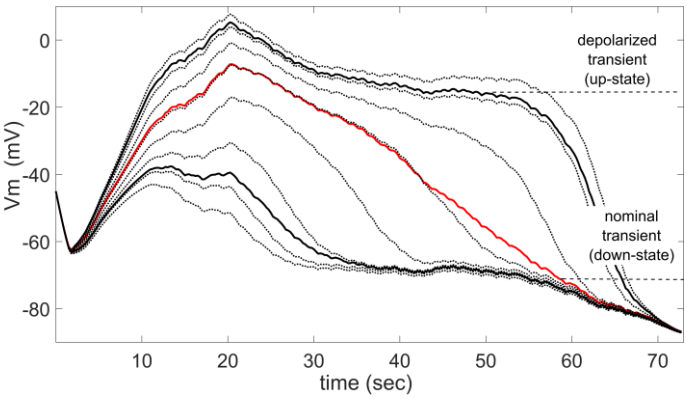

Figure 10 – Glial switching between down-state and up-state was robustly observed for parameters in the bistability range of the resting state(s) in simulations of the model (13), perturbed with a seizure-like transient, Fig. 9. Dotted lines show ten simulations for $0.01 < g_{lfp} < 0.0155\ \mu S$. To verify the parameter ranges are robust to fluctuations, we randomized $(g_{lfp},\ g_{s-inw})$ values in ten runs of the three qualitatively different responses within 10% of their indicative ranges and averaged them, bold black lines. The up-state and down-state are separated by a separatrix response that does not follow the perturbing waveform. Varying I_{gjc}, g_{leak} and nominal $[K^+]_o$ change the threshold and waveform but the two-plateau response typically remains for I_{gjc} in bistability range.

The asymmetry of the division of g_{lfp} range reflects the position of the saddle point V_s between the two stable nodes (V_r and V_{dr}), Fig.6B, or in other words, the position of the stable manifold of the saddle V_S, which is the true separatrix in the phase plane.

4. Discussion / I ~ *importance*, S – *significance*, N – *novelty*, U - *utility* /

The observed dynamical instability could point to different areas of impact depending on the physical model system and the specific V_m dependence of the modeled phenomenon. A general conclusion in hypothesis-free biophysical terms would be that with its very basic ion channel composition the glial membrane responds differently and distinctly to external depolarizations when Kir or combinations of Kir and K2P conductances are deregulated, due to the interplay of Ohmic and complex non-Ohmic conductances, nonlinear in V_m. Below, we discuss the possible implications of the presented biophysics from several different neurobiological perspectives.

(I1) There have been numerous *association studies* where changes in expression of Kir4.1 currents and the biophysical properties of measured macroscopic currents have been related, *put in context*, to the altered function of glia. In translating such changes into specific roles of the cell, it has remained elusive which mechanisms could transduce the molecular changes into a whole-cell response. We modeled V_m dynamic of an isolated astrocyte by a minimal ODE model incorporating the major K^+conductances, WR-Kir and K2P, and a leak current to explore the direct effect of nonlinear changes in the total astrocytic ion conductance to V_m dynamics. In other words, it models the simplest form of modulation of V_m by alterations of ion conductances with no other signal transductions being modeled, like membrane mechano-sensitivity, pH sensitivity, actions of physiological agonists, etc. The main question in the stability analysis of (13), is which nature of (de)regulation of the whole-cell conductance impacts the stability of the nominal resting state V_r, which in turn controls all electrogenic transport mechanisms.

(I2) Decades of modeling using Hodgkin-Huxley conductance-based models suggest that even very small currents should be carefully considered since the nonlinear interplay of their conductances could change the stability of the resting state and in turn the cell response (Izhikevich, 2007). That has motivated the incorporation of the K2P current through its activation dynamics, $n(t)$, as a second dynamical variable. The necessary model perturbations came from decreased Kir conductance in the outward V_m range, with K2P conductance remaining unchanged or eventually increased, resulting in a non-monotonic steady-state I-V curve. **(N1)** In that regard we present the

first ODE model of glial V_m (13) where two distinct and *differentially regulated* K^+currents, in addition to the unspecific K^+leak current, have been incorporated based on recordings from isolated cells.

(S1) Non-monotonous, N-shaped I-V relation produced by a prominent decrease of WR-Kir in the outward range, gives birth to a new, much more depolarized *stable* steady state V_{dr} for a physiological range of average external depolarizing current, I_{ext}. When present, such a mathematical feature of a model of a non-excitable cell is generic and observed robustly in a wider parameter range, Fig. 7. We argue here that the emergence of a distinct and stable V_{dr} introduces a specific and distinctive transition - translating the loss of pseudo-Ohmic, linear behavior of the membrane into a *bistable switch* when exposed to depolarizing transients, Fig. 9. It would be unrealistic and insignificant to demonstrate that switching between V_r and V_{dr} is plausible in real glial cells by simulating the model using strong constant current perturbations I_{ext}, since glial cells in real circuits do not receive prolonged depolarizations by constant external currents. The initial, steady depolarizing phase of the realistic V_m transient we used in (15), the first ten seconds before the clonic phase (Traynelis & Dingledine, 1988), is critical for the switching between the up-state and down-state to be observed and we believe has a typical waveform for a wider range of strong transient depolarizations resulting from local neuronal synchrony.

(S2), (N2) Translating V_m bistability and altered WR-Kir current into effects significant for the whole cell function, the following impacts are directly implicated by the model:

- **Depolarized resting state V_{dr} as a *catastrophic event*[5]** – Even though it is one of the few primitive instability scenarios, the birth of a stable, very depolarized resting state is potentially *catastrophic* since switching to $V_{dr} > -10\ mV$ is taking the membrane and the cell, to a state with much higher potential energy than the nominal hyperpolarized resting state, not corresponding to the actual $[K^+]_o$. Prolonged depolarization of the glial membrane around V_{dr} would impact all glial functions, from metabolic support to membrane transport, and practically all neuromodulatory roles assigned to glia.
- **(I3) Voltage switching between V_r and V_{dr} disrupts the kinetics of active ion and other transport mechanisms nominally running near V_r** - Since all major electrogenic pumps and transporters show some extent of voltage dependence (De Weer, Gadsby, & Rakowski, 1988), (Läuger, 1984), (Poulsen, Morth, Egebjerg, & Nissen, 2010), the depolarized V_{dr}, or the up-state should violate the assumptions made for the steady-state transport rates near V_r. In the case of ATP-driven pumps, in the Na-K pump, for example, all simplified descriptions used in computational models, in a form of a simple current generator $I_{pump} = \rho f([K^+]_o, [Na^+]_i)$ focusing on the "acceleration" term f which models the sensitivity to ion concentration changes, are warranted by the existence of a constant steady-state rate ρ, assumed to be voltage-independent. When V_m switches to $V_{dr} > -10\ mV$, dramatically shifted ΔV_m to large positive values impacts some of the binding and translocation steps in the kinetic model of the pump and questions the biophysical plausibility of keeping ρ constant. In particular, in cases where the perturbing voltage transient like the electrographic seizure we used, produces a jump near V_{dr} *not resulting* from moderately elevated $[K^+]_o$, i.e. E_K not much above V_r, a large and lasting positive transient is produced. If further studies prove the bistability in V_m is electrophysiologically plausible, moving to a more detailed macroscopic model of the pump might be required with ρ explicitly depending on the full form of the electrochemical potential. For the pump rate ρ in units of molar flux, we can write (Läuger, 1984):

$$\rho \sim \Delta G + \Delta\tilde{\mu}_H\ \ (mM/s), \quad \text{where } \Delta\tilde{\mu}_H = \Delta\mu + zFV_m\ \ (RT\ units),$$
$$RT\ln(c_{ext}/c_{in}) + zFV_m < -\Delta G, \ \text{for active transport,} \qquad (16)$$

[5] We use the term in the context of the *catastrophe theory* of dynamical systems (Gilmore, 1993), (Zeeman, 1977) and *catastrophic bifurcations* (Abraham & Shaw, 1982), initially formulated over the impact of the same instability we observed - the fold bifurcation, on the global behavior of both, natural and man-made systems.

where ΔG represents the purely chemical potential energy from ATP hydrolysis, and within the electrochemical part $\Delta\tilde{\mu}_H$we recognize the Nernstian, or osmolar contribution $\Delta\mu = RT\ln(c_{ext}/c_{in})$ and the electrical part zFV_m that impacts ρ under prolonged depolarization at V_{dr}. An implicit assumption not typically discussed is that only near the nominal equilibrium V_r where the electrochemical gradient ΔV_m is small and the osmolar contribution large and steady, the FV_m term could be eventually neglected. The inequality in (16) is the typical condition for a sustained primary active transport, with sign convention in $-\Delta G$ representing the amount of free energy available from hydrolysis of a mole ATP, rather than the barrier height in the enzymatic reaction (Adam, 2009), (Läuger, 1984). Some variants of the macroscopic model of the pump have kept the voltage dependence (Forrest, 2014) and have produced effects in whole-cell dynamics attributable to the Na-K pump. In such models, the eventual effects of voltage bistability could be directly tested. Stoichiometry coefficients have been omitted in (16) for simplicity.

The electrogenic sodium bicarbonate Na^+/HCO_3^- cotransporter (NBCe1) specifically implicated in glial metabolic and other functions, is another important candidate to be analyzed in the context of bistability since the reversal of the polarity of ΔV_m would cause switching of the transport direction and in turn the whole-cell mode between alkalization and acidification of the cell itself, and consequently the immediate extracellular environment (Ransom, 2000).

Of the other transporters potentially "vulnerable" to bistability let us mention the astrocytic GABA transporters (GAT1-GAT3) expressed in local cortical circuits (Fattorini, Melone, & Conti, 2020), (Zafar & Jabeen, 2018), modeled macroscopically as explicitly V_m dependent (Hoshino, Kameno, Kubo, & Watanabe, 2020).

- **(I4)**, **(S3) Glial encoding of $[K^+]_o$ variations as a signal gets a distinct state** – In the present understanding of the *encoding capability* of glial membrane, the glial V_m with certain low-pass filtering capability (with $\tau_m = C_{eff}/g_{slope} \approx 10ms$ for 20pF patch capacitance) close to linearly encodes $[K^+]_o$variations as a signal through $(V_m - E_K)$. We can also say E_K itself smooth out the real-time K^+ variations from neuronal discharging partly due to the low-pass filtering of the ECS to volume transmission signals (Bedard et al., 2006) and partly due to the $\log(c_{out}/c_{in})$ nature of Nernstian dependence. The emergence of V_{dr} introduces therefore a distinct, depolarized state potentially detectable on various timescales by a suitable measurement setup. In other words, V_r and V_{dr} encode the (a) almost linear potassium electrode, and (b) the deformed, N-shaped I-V relationship of the deregulated membrane, respectively, Fig. 6A.
- **(I5)**,**(S4) Switching between the two resting states may introduce erratic transients in trans-junctional voltage over the GJCs –** It has been shown that the conductance and rectification of GJCs are dependent on the trans-junctional voltage V_J between the connected cells across a wide range of the Connexin isoforms (Bargiello et al., 2018), (Oh, 2015), (Maciunas, Snipas, Paulauskas, & Bukauskas, 2016), and specifically for the Connexin43 hemichannels, one of the two most abundant subtype assembling the astrocytic GJCs, with Connexin30 (Bukauskas, Bukauskiene, & Verselis, 2002). In addition to the nonlinear steady-state I-V relationship of the GJ connections and $g_{gjc}(V_J)$ dependence of the conductance, the complex two-stage gating in most of the hemichannles may result in erratic behavior of the GJC if the connected cells are prone to switching between V_r and V_{dr}. Atomic level model of GJC electrostatics (Escalona et al., 2016) suggests complex Coulombic profiles potentially vulnerable to erratic V_J and V_m switching on multiple positions. The resulting V_J and $V_m$switching may keep both, the hemichannel and the GJC dwelling in an unstable state between the residual and fully conductive conformations, or depending on the frequency of bistability switching between the *instantaneous and steady* $g_{gjc}(V_J)$ which could be markedly different (Oh, 2015). Even though massive glial disconnection is a proven hallmark of chronic epilepsies (Bedner et al., 2015), (Binder & Steinhauser, 2021) eventual

causative role of GJC failure is yet to be shown pointing eventually to the biophysical mechanism.

In the case of open, background Kir channels we departed from the typical modeling approach, a single current – single biophysical description. The reversal of polarity of the driving force changes the nature of the physiological block resulting in **qualitatively different pseudo-gating in the WR-Kir pore for inward and outward flux** (Appendix A). This assumption warrants to use two different biophysical descriptions for additive inward and outward fluxes. Figure 3 suggests that this conceptual approach results in an overlapping $V_m$regions where both mechanisms (blue and red curve in Fig.3) produce a small outward current. Those outward permeation events happen for very small ΔV_m where the electrical enthalpic contributions are comparable to the fluctuations – resulting in outward pseudo-gating in both, the central cavity, as well as within the SF, described respectively by the Hagiwara model, and by the extended, non-classical GHK equation (5). Such different gating scenarios require several effective charge valences z_{inw}, z_B, and z to appear within descriptions of WR-Kir current.

(N3) Departing from the constant field assumption in the Nernst-Planck formalism of an open pore, results in a modified Goldman-Hodgkin-Katz current equation which allows incorporating simple forms of nonlinear energy profiles $U(x)$ within the pore, as long as the integral in the current equation is solvable (Jackson, 2006). We applied it for the first time to describe the outward component of WR-Kir current (8), and by extending it with quadratic dependence of the barrier peak (7), the observed current saturation with voltage was captured by the model, Fig. 4. Accumulating evidence of complex gating in open pores, that does not express a voltage-sensitive gate, may qualify this approach in a wide range of leaky channels.

In summary, the proposed minimal 2-dimensional model of the interplay between WR-Kir and K2P currents in astrocytic membrane shows that deregulations turning WR-Kir current into inwardly rectified, robustly produce a second very depolarized steady state of V_m and a whole-cell behavior considered markedly non-physiological within glial biology. To prove or refute such bistability as neurobiologically plausible, a measurement protocol well suited for transient V_m changes would be needed, probably employing voltage imaging, a dynamic (current) clamp, and cell assays displaying deregulated Kir4.1 or sufficient densities of Kir4.1/Kir5.1 channels of glial origin.

Preliminary extension of (13) we attempted with $[K^+]_o$ dynamics (Barreto & Cressman, 2011), (Cressman, 2009), (Krishnan, Filatov, Shilnikov, & Bazhenov, 2015) *in a very simplified, spatially constraint ECS* compartment demonstrated enriched dynamical repertoire of the model and will be reported in another study. Within $[K^+]_o$ ranges indicating the richer bifurcation repertoire in (Barreto & Cressman, 2011) and (Erhardt, Mardal, & Schreiner, 2020), we observed some entrainment of the glial V_m in (13) by the $[K^+]_o$dynamics driven by the neuronal bursting (Barreto & Cressman, 2011), but those require more precise dynamical characterization. Other important extensions of the model should include (a) incorporating the chloride conductances explicitly and (b) adding mechanosensitivity to K2P conductances to simulate the osmolar stress of the membrane.

Very limited availability of transient recordings from glia leaves us without traces of real-time perturbations of glial V_m on different time scales which is a limiting factor to considering a non-autonomous, driven form of the model (13), since in immediate proximity of spiking neurons the glial cells are never in a true voltage steady state. The heavily interconnected glial cells in the *glial cell continuum* require testing any indications of V_m multistability using boundary value problem models in the light of experimentally observed V_m *isopotentiality* (Ma, 2016).

The presumed ion-homeostatic role of Kir4.1 in glia was not discussed in the context of bistability because the differential contributions of the different ion transport mechanisms are still elusive (MacAulay, 2020), and reasonably minimal mathematical model addressing the spatial complexity of volume transmission in neuroglial circuits requires a dedicated experimental study.

(U1) The proposed model (13) is of general biophysical utility, directly applicable to the interplay between Kir and K2P currents in membranes of other systems where K2P channel variants display nonnegligible activation kinetics, like in the heart and kidneys, see (Sepúlveda, 2015) for more

cases. Bistability showing comparable voltage separation of V_r and V_{dr} like presented has been already observed in cardiomyocytes in hypokalemic conditions (Zuo, 2017), where strongly-rectifying Kir2.1 channels interwork with the linear K2P-TWIK channels.

Acknowledgments – We thank Prof. Christian Steinhäuser and Dr. Gerald Seifert for sharing with us the unique recordings from isolated astrocytes (Seifert et al., 2009) of both Kir and K2P currents, for their lasting support in getting a sense of data and experimental limitations, as well as to CS on the numerous discussions and critical inputs. We thank Prof. Meyer Jackson for his comments on the model of I_{res} current, and for his inspiring treatment of biophysics of open pores (Jackson, 2006) which motivated our modeling on several points. We thank Prof. Pavle Andjus for his comments on the simulation results. This study was partly funded by the National Institute of Mental Health (US), grant numbers MH117769 and MH125030 to PJ.

The XPPAUT .ode files for the bifurcation analysis and simulations will be available in *ModelDB* at https://senselab.med.yale.edu/ModelDB, under the model name "*Glial voltage dynamics driven by Kir & K2P currents*".

Appendix-1 Short-pore model of WR-Kir channel and physiological Mg^{2+} block

We base our biophysical reasoning on (i) conduction phenomena through a *short pore* (Fig. A1), common to all K^+ channels - confined to the part of the transmembrane structure consisting of a selectivity filter (SF) and internal water-filled *central cavity* (Doyle et al., 1998), (Allen, Bliznyuk, Rendell, Kuyucak, & Chung, 2000) and on (ii) *physiological blocking* of the pore by cytoplasmic cations as a permeability control mechanism. Coulombic interactions within the short pore are therefore used to explain the permeation mechanisms as an interaction between the blocking Mg^{2+} and permeant K^+ ions, as a basis for a weak rectification. Unlike in strong inward rectification, where both, the internal Mg^{2+} and polyamines fully block outward flux (Lu, 2004), (Matsuda, 1991), in the outward permeation scenario of a weakly rectifying pore (Fig. A1C) the partial and flickering block allows the entrance of permeant ions into the SF at high rates. This pore model is crucial for explaining the *anomalous*, inward rectification of K^+ conductivity, which can't be described by Nernst-Planck (NP) formalism based on electrochemical gradients over open, leaky channels. The short pore model applied to outward conduction in WR-Kir channels, allows extending the NP model with a non-constant field and in turn a voltage-dependent permeability, equation (9), under the assumptions of a changing Coulombic profile with voltage. These extensions formulate the main assumptions of the I_{res} model (Jackson, 2006).

Recent evidence from single-channel recordings and molecular dynamics simulations of the potassium KcsA pore (Heer, 2017) suggests that the voltage and ligands induce *structural fluctuation* changes within the electrostatics, Coulombic profile of SF which produces a universal pseudo-gating of an open pore at SF, *without* introducing a conformational change and gating.

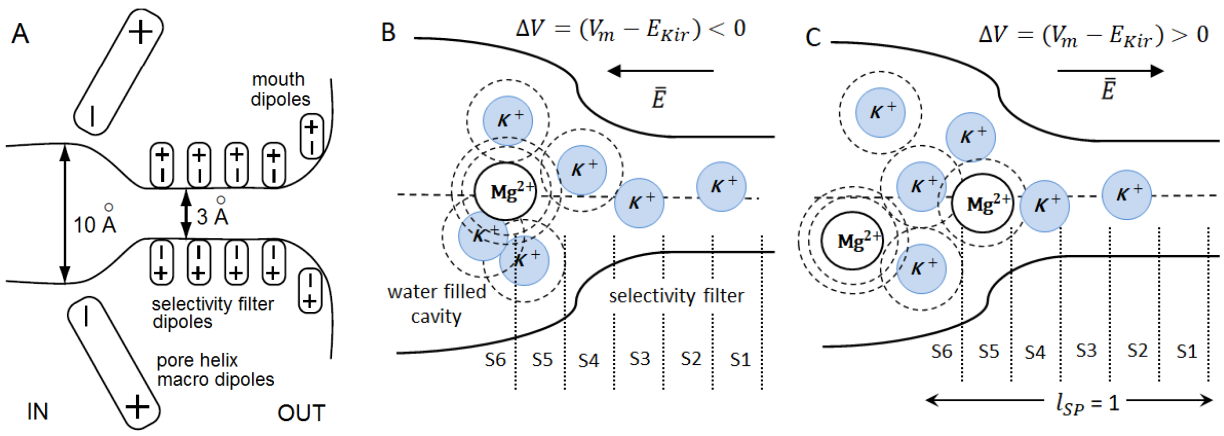

Figure A1 - S*hort pore* model of permeation through generic weakly-rectifying Kir channels – **(A)** A *short-pore* view of the Kir pore consisting of a selectivity filter (SF) and the inner, water-filled *central cavity*. The sketch shows the sources of electrostatic interaction along with the transmembrane structure acting on permeant and blocking ions, modified from (Jackson, 2006). Inside the SF, selectivity filter dipoles create binding sites (S1 to S4), corresponding to energy wells where permeant ions are stabilized between the transitions. (**B**) and (**C**), a simplified one-dimensional view of the short pore, outline the *different* voltage dependence of Mg^{2+} block and the Coulombic interaction with the permeant ions. From negative to positive $\Delta V_m = (V_m - E_{Kir})$, and constant or slowly varying $[K^+]_o$, the resulting force on $Mg^{2+}$and K^+ions changes and the resulting blocking events are qualitatively different, see text for details. Arrows show the direction of the electrical field $\bar{E}$ on a positive ion, in a simplified one-dimensional reaction coordinate. We assign a unitary length l_{SP} (shown in C) to the extent of the pore over which we model potential energy landscape. Dashed circles around the ions in (B) and (C) represent the full or partial hydration shells. The length of the SF without the outer vestibule in (B) and (C) is disproportionally shorter than in (A), to keep the image compact.

The short-pore model assumes the concentration of $Mg^{2+}$and K^+within the central cavity and at the external pore vestibule, correspond to the physiological intracellular and extracellular bath concentrations respectively. Local, *relative, nonequilibrium concentration changes* due to effects like the attraction of cations by rings of negatively charged residues, in vestibules on either side of the SF entrance, are neglected.

We assume that the transmembrane voltage V_m drops only over *short pore,* mainly along the cavity and the SF, from S1 to S5 (which corresponds to the *fractional electrical distance* $= 1$), influencing with a smaller fraction the S5 position, marked δV_m on Fig.3. S0 indicates a position just outside the SF, in the outer vestibule (Fig. A1B and A1C). This is a similar approach to the one used in permeation studies of weak rectification in renal Kir1.1 / ROMK1 (Yang, Edvinsson, Sackin, & Palmer, 2012b; Yang, Edvinsson, Sackin, & Palmer, 2012a). This pore model suggests that the blocking cation moves between two *modulatory* sites (B. Hille, Schwartz, W, 1978) depending on ΔV_m polarity, thereby defining the main rectification barrier(s).

Inward pseudo gating - For negative and very small positive net driving forces ΔV_m, (Fig. A1B), the resulting electrostatics from pore helix macro dipoles keeps blocking Mg^{2+}ions within the cavity (designated by position S6), so that the inward rectification results from a competition of permeant K^+ and Mg^{2+} ions for the central, axial positions within the cavity. Even though V_m influences S6 position with a much smaller fraction δV_m (Fig. 3) the dependence of inward flux on V_m for $\Delta V_m < 0$ is still exerted on the K^+ion in S6 by the multi-ion file within SF (binding positions S1 to S4), which contributes to the resulting Coulombic forces and ion-crowding within the central cavity (represented by S5 and S6 positions). By resulting force, in this simplified view, we mean Coulombic repulsion between the permeant ions acting in parallel to the stabilizing attractive force on them coming from the negative end of pore helix macro dipoles (Fig. A1A), tilted so to make the center of the cavity electrostatically favorable point for a cation (B. Hille, 2001). Hagiwara's measurements of macroscopic Kir currents demonstrated the existence of equilibrium pore-open probabilities of the *inwardly permeant* pore in Kir channels, suggesting the Boltzmann term in the Hagiwara model (3) for a description of macroscopic conductance, similar to open and closed probability in gated ion channels, see (Lu, 2004) for Kir-specific review.

Outward pseudo gating - In the reverse case, for a more positive driving force $V_m > -50mV$ (Fig. A1C), an outwardly directed net driving force acts on permeant and blocking cations, pushing partly or fully dehydrated Mg^{2+}ion towards the entry of the SF, which results in a partial flickering plug of the pore at the S5 site. Blocking ion at S5 creates the entry barrier to the permeant ion, $\lambda_1$wide in units of fractional electrical distance (Fig. A1C), extending through S4 and S3 positions.

The different nature of the resulting electrostatics in these two cases implicates different permeation mechanisms and warrants the use of a different biophysical description of unidirectional fluxes. We, therefore, model the unidirectional fluxes as additive over the whole V_m range of the measured Kir4.1 current. In other words, the proposed modeling approach suggests *that in its structure-function a weak rectifier results as a superposition of inward and outward rectifiers*. Single mutation studies (Wible et al., 1994), (Lu Z., 1994) suggested the structural determinants are very similar and a single point mutation flips the pore from a strong Kir2.1 to a weak Kir1.1 rectifier.

Appendix-2

Table 2 - Experimental studies reporting altered properties of Kir4.1 current

Altered current	Exp. Model, Reference	WR-Kir inward	WR-Kir outward	Cell type	Comment
Kir4.1 current	Astrocytes in ALS (Bataveljić, 2012)	↓↓	↓↓	Astrocytes in culture	Non-Kir outward current increased markedly in the ALS model
Kir4.1 outward current	Astrocytes in Huntington's Disease (Tong, 2014)	↓	↓↓↓	Astrocytes in slices	
Currents through the heteromerric Kir4.1/Kr5.1 channels	(Marmolejo-Murillo et al., 2021)	Not altered	Abolished	HEK-293 cells	Kir channels introduced by DNA transfection
Kir4.1 currents	Astrocytes in Depression (Cui, 2018)	↑↑	↑↑↑	Astrocytes in slices	Not considered in the parametric analysis since the I-V curve remains monotonic.

References

Abraham, R., & Shaw, C. D. (1982). *Dynamics-the geometry of behavior - Part Four: Bifurcation Behavior*. Santa Cruz, Calif.: Aerial Press.

Adam, G., Läuger, P., and Stark, G. (2009). *Physikalische Chemie und Biophysik*: Springer-Verlag.

Allen, T. W., Bliznyuk, A., Rendell, A. P., Kuyucak, S., & Chung, S.-H. (2000). The potassium channel: Structure, selectivity and diffusion. *J Chem Phys, 112*, 8191-8204.

Ballanyi, K., Grafe, P., & ten Bruggencate, G. (1987). Ion activities and potassium uptake mechanisms of glial cells in guinea-pig olfactory cortex slices. *J. Physiol, 328*, 159-174.

Bargiello, T. A., Oh, S., Tang, Q., Bargiello, N. K., Dowd, T. L., & Kwon, T. (2018). Gating of Connexin Channels by transjunctional-voltage: Conformations and models of open and closed states. *Biochim. Biophys. Acta, 1860*, 22–39.

Barreto, E., & Cressman, J. (2011). Ion concentration dynamics as a mechanism for neuronal bursting. *J Biol Phys, 37*, 361–373.

Bataveljić, D., Nikolić L., Milošević M., Todorović N., Anđus P.R. (2012). Changes in the astrocytic aquaporin-4 and inwardly rectifying potassium channel expression in the brain of the amyotrophic lateral sclerosis SOD1(G93A) rat model. *GLIA, 60*(12), 1991–2003.

Bedard, C., Kroger, H., & Destexhe, A. (2006). Model of low-pass filtering of local field potentials in brain tissue. *Physical Review E, 73*(5).

Bedner, P., Dupper, A., Huttmann, K., Muller, J., Herde, M. K., Dublin, P., . . . Steinhäuser, C. (2015). Astrocyte uncoupling as a cause of human temporal lobe epilepsy. *Brain, 138*, 1208–1222.

Bedner, P., Jabs, R., & Steinhäuser, C. (2019). Properties of human astrocytes and NG2 glia. *GLIA, 68*, 756-767.

Benbow, S. J. (2020). *Graph Grabber* (Version 2.0.2): Quintessa, Henley-on-Thames, United Kingdom. Retrieved from https://www.quintessa.org/software/downloads-and-demos/graph-grabber-2.0.2

Binder, D. K., & Steinhauser, C. (2021). Astrocytes and Epilepsy. *Neurochem Res, 46*(10), 2687-2695. doi:10.1007/s11064-021-03236-x

Borg-Graham, L. (1999). Interpretations of Data and Mechanisms for Hippocampal Pyramidal Cell Models. In *Cerrebral Cortex - Models of Cortical Circuits* (Vol. 13, pp. 19-137). New York: Springer Science.

Bukauskas, F. F., Bukauskiene, A., & Verselis, V. K. (2002). Conductance and permeability of the residual state of connexin43 gap junction channels. *J Gen Physiol, 119*(2), 171-185. doi:10.1085/jgp.119.2.171

Chen, H., Zuo, D., Zhang, J., Zhou, M., Ma, L. (2014). Classification of 2-pore domain potassium channels based on rectification under quasi-physiological ionic conditions. *Channels, 8*, 503-508.

Cressman, J., Ullah, G., Ziburkus, J., Schiff, SJ., Barreto, E. (2009). The influence of sodium and potassium dynamics on excitability, seizures, and the stability of persistent states: I. Single neuron dynamics. *J Comput Neurosci, 26*, 159–170.

Cui, Y., Yang, Y., Ni, Z., Dong, Y., Cai, G., Foncelle, A., Ma, S., Sang, K., Tang, S., Li, Y., Shen, Y., Berry, H., Wu, S., Hu, H. (2018). Astroglial Kir4.1 in the lateral habenula drives neuronal bursts in depression. *Nature, 554*, 323–327.

De Weer, P., Gadsby, D. C., & Rakowski, R. F. (1988). Voltage dependence of the Na-K pump. *Annu Rev Physiol, 50*, 225-241.

Destexhe, A., Huguenrad, J.,. (2000). Nonlinear Thermodynamic Models of Voltage-Dependent Currents. *J Comp Neurosci, 9*, 259–270.

Doedel, E., Champneys , A. R., Fairgrieve , T. F., Kuznetsov, Y. A., Sandstede , B., & Wang, X. (1997). AUTO 97: Continuation and bifurcation software for ordinary differential equations (with HomCont): indy.cs.concordia.ca.

Doyle, D. A., Morais Cabral, J., Pfuetzner, R. A., Kuo, A., Gulbis, J. M., Cohen, S. L., . . . MacKinnon, R. (1998). The Structure of the Potassium Channel: Molecular Basis of K+ Conduction and Selectivity. *Nature, 280*, 69-77.

Edvinsson, J., Shah, AJ., Palmer, LG.,. (2011). Kir4.1 K+ channels are regulated by external cations. *Channels (Austin)*, 5(3):269-279.

Eisenman, G., Horn, R. (1983). Ionic selectivity revisited: The role of kinetic and equilibrium processes in ion permeation through channels. *J Membrane Biol, 76*(3), 197–225.

Enyedi, P., & Czirjak, G. (2010). Molecular background of leak K+ currents: two-pore domain potassium channels. *Physiol Rev, 90*(2), 559-605. doi:10.1152/physrev.00029.2009

Erhardt, A. H., Mardal, K. A., & Schreiner, J. E. (2020). Dynamics of a neuron-glia system: the occurrence of seizures and the influence of electroconvulsive stimuli : A mathematical and numerical study. *J Comput Neurosci, 48*(2), 229-251. doi:10.1007/s10827-020-00746-5

Ermentrout, B. (2002). *Simulating, analyzing, and animating dynamical systems: a guide to XPPAUT for researchers and students*. Philadelphia: Society of Industrial and Applied Mathematics (SIAM).
Escalona, Y., Garate, J. A., Araya-Secchi, R., Huynh, T., Zhou, R., & Perez-Acle, T. (2016). Exploring the Membrane Potential of Simple Dual-Membrane Systems as Models for Gap-Junction Channels. *Biophys J, 110*(12), 2678-2688. doi:10.1016/j.bpj.2016.05.005
Fattorini, G., Melone, M., & Conti, F. (2020). A Reappraisal of GAT-1 Localization in Neocortex. *Front Cell Neurosci, 14*, 9. doi:10.3389/fncel.2020.00009
Felix, L., Delekate, A., Petzold, G. C., & Rose, C. R. (2020). Sodium Fluctuations in Astroglia and Their Potential Impact on Astrocyte Function. *Front Physiol, 11*, 871. doi:10.3389/fphys.2020.00871
Forrest, M. D. (2014). The sodium-potassium pump is an information processing element in brain computation. *Front Physiol, 5*, 472. doi:10.3389/fphys.2014.00472
Gilmore, R. (1993). *Catastrophe theory for scientists and engineers*. New York: Dover Publications.
Gonzalez, C., Baez-Nieto, D., Valencia, I., Oyarzun, I., Rojas, P., Naranjo, D., & Latorre, R. (2012). K(+) channels: function-structural overview. *Compr Physiol, 2*(3), 2087-2149. doi:10.1002/cphy.c110047
Hagiwara, S., and, & Takahashi, K. (1974). The Anomalous Rectification and Cation Selectivity of the Membrane of a Starfish Egg Cell. *J. Membrane Biol., 18*, 61-80.
Hebert, S., Desir, G., Giebisch, G., Wang, W. (2005). Molecular Diversity and Regulationof Renal Potassium Channels. *Physiol Rev, 85*, 319 –371.
Heer, T. H., Posson, D.J., Wojtas-Niziurski, W., Nimigean, C.M., Bernèche, S. (2017). Mechanism of activation at the selectivity filter of the KcsA K+ channel. *eLife*, 6:e25844.
Henneberger, C., & Rusakov, D. (2012). Monitoring local synaptic activity with astrocytic patch pipettes. *Nature Protocols, 7*, 2171-2179.
Hibino, H., Fujita, A., Iwai, K., Yamada, M., & Kurachi, Y. (2004). Differential assembly of inwardly rectifying K+ channel subunits, Kir4.1 and Kir5.1, in brain astrocytes. *J Biol Chem, 279*(42), 44065-44073. doi:10.1074/jbc.M405985200
Hibino, H., Inanobe, A., Furutani, K., Murakami, S., Findlay, I., & Kurachi, Y. (2010). Inwardly rectifying potassium channels: their structure, function, and physiological roles. *Physiol Rev, 90*(1), 291-366. doi:10.1152/physrev.00021.2009
Hille, B. (2001). *Ionic Channels of Excitable Membranes, 3rd Ed.* Sunderland, MA: Sinauer Associates Inc.
Hille, B., Schwartz, W. (1978). Potassium Channels as Multi-Ion Single-file Pores. *J Gen Physiol, 72*, 409-442.
Hodgkin, A. L., & Horowicz, P. (1959). The influence of potassium and chloride ions on the membrane potential of single muscle fibres. *J. Physiol, 148*, 127-160.
Honore, E. (2007). The neuronal background K2P channels - focus on TREK1. *Nat. Rev. Neurosci., 8*, 251-261.
Hoshino, O., Kameno, R., Kubo, J., & Watanabe, K. (2020). Spatiotemporal regulation of GABA concentration in extracellular space by gliotransmission crucial for extrasynaptic receptor-mediated improvement of sensory tuning performance in schizophrenia. *J Comput Neurosci, 48*(3), 317-332. doi:10.1007/s10827-020-00755-4
Izhikevich, E. M. (2004). Which model to use for cortical spikin neurons? *IEEE Trans Neural Networks, 15*(5), 1063 - 1070.
Izhikevich, E. M. (2007). *Dynamical Systems in Neuroscience - The Geometry of Excitability and Bursting*. Cambridge, Massacusetts: The MIT Press.
Jackson, M. B. (2006). *Molecular and Cellular Biophysics*. New York: Cambridge Univ. Press.
Johnston, D. a. W., S.M-S. (1995). *Foundations of Cellular Neurophysiology*. Cambridge, Massachusetts: The MIT Press.
Kettenmann, H., Backus, K. H., & Schachner, M. (1984). Aspartate, glutamate and γ-aminobutyric acid depolarize cultured astrocytes. *Neuroscince Letters, 52*, 25-29.
Kettenmann, H., & Steinhäuser, C. (2005). Receptors for neurotransmitters and hormones. In H. Kettenmann, and Ransom, BR., (Ed.), *Neuroglia* (pp. 131-145). New York: Oxford University Press.
Krishnan, G. P., Filatov, G., Shilnikov, A., & Bazhenov, M. (2015). Electrogenic properties of the Na(+)/K(+) ATPase control transitions between normal and pathological brain states. *J Neurophysiol, 113*(9), 3356-3374. doi:10.1152/jn.00460.2014
Kubo, Y., Baldwin, T. J., Jan, Y. N., & Jan, L. Y. (1993). Primary structure and functional expression of a mouse inward rectifier potassium channel. *Nature*, 362:127-133.
Kuffler, S., Nicholls, J. G., & Orkand, R. (1966). Physiological properties of glial cells in the central nervous system of amphibia. *J Neurophysiol, 26*, 768-787.
Kurata, H. T., Rapedius, M., Kleinman, M. J., Baukrowitz, T., & Nichols, C. G. (2010). Voltage-dependent gating in a "voltage sensor-less" ion channel. *PLoS Biol, 8*(2), e1000315. doi:10.1371/journal.pbio.1000315

Läuger, P. (1984). Thermodynamic and kinetic properties of electrogenic ion pumps. *Biochem Biophys Acta, 779*, 307-341.
Lu, Z. (2004). Mechanism of Rectification in Inward-Rectifier K+ Channels. *Annual Rev Physiol*, 66:103-129.
Lu Z., M., R. (1994). Electrostatic tuning of Mg2+ affinity in an inward-rectifier K+ channel. *Nature*, 371:243-245.
Ma, B., Buckalew, R., Du, Y., Kiyoshi, CM., Alford, CC., Wang, W., McTigue, DM., Enyeart JJ., Terman D., Zhou M.,. (2016). Gap junction coupling confers isopotentiality on astrocyte syncytium. *GLIA, 64*, 214-226.
MacAulay, N. (2020). Molecular mechanisms of K(+) clearance and extracellular space shrinkage-Glia cells as the stars. *GLIA, 68*(11), 2192-2211. doi:10.1002/glia.23824
Maciunas, K., Snipas, M., Paulauskas, N., & Bukauskas, F. F. (2016). Reverberation of excitation in neuronal networks interconnected through voltage-gated gap junction channels. *J Gen Physiol, 147*(3), 273-288. doi:10.1085/jgp.201511488
Marcus, R. (1964). Chemical and Electrochemical Electron-Transfer Theory. *Annu. Rev. Phys. Chem., 15*, 155-196.
Marmolejo-Murillo, L. G., Arechiga-Figueroa, I. A., Moreno-Galindo, E. G., Ferrer, T., Zamora-Cardenas, R., Navarro-Polanco, R. A., . . . Rodriguez-Menchaca, A. A. (2021). Kir4.1/Kir5.1 channels possess strong intrinsic inward rectification determined by a voltage-dependent K+-flux gating mechanism. *J Gen Physiol, 153*(5). doi:10.1085/jgp.201912540
Matsuda, H. (1991). Effects of external and internal K+ ions on magnesium block of inwardly rectifying K+ channels in guinea-pig heart cells. *J.Physiol*, 435:483.
Matyushov, D. V. (2015). Protein electron transfer: is biology thermodynamic? *J Phys Condens Matter, 27*(47), 473001.
Meeks, J. P., & Mennerick, S. (2007). Astrocyte membrane responses and potassium accumulation during neuronal activity. *Hippocampus, 17*(11), 1100-1108. doi:10.1002/hipo.20344
Oh, S., and Bargiello, T.,. (2015). Voltage Regulation of Connexin Channel Conductance. *Yonsei Med J, 56*, 1-15.
Ohmori, H. (1978). Inactivation kinetics and steady-state current noise in the anomalous rectifier of tunicate egg cell membranes. *J.Physiol.*, 281:277–299.
Peters, B. (2015). Common features of extraordinary rate theories. *J Phys Chem B, 119*(21), 6349-6356. doi:10.1021/acs.jpcb.5b02547
Poulsen, H., Morth, P., Egebjerg, J., & Nissen, P. (2010). Phosphorylation of the Na+,K+-ATPase and the H+,K+-ATPase. *FEBS Lett, 584*(12), 2589-2595. doi:10.1016/j.febslet.2010.04.035
Ransom, B. R. (2000). Glial modulation of neural excitability mediated by extracellular pH: a hypothesis revisited. *Prog Brain Res, 125*, 217-228. doi:10.1016/S0079-6123(00)25012-7
Ransom, B. R., & Goldring, S. (1973). Ionic determinants of membrane potential of cells presumed to be glia in cerebral cortex of cat. *J Neurophysiol, 36*(5), 855-868. doi:10.1152/jn.1973.36.5.855
Schewe, M., Nematian-Ardestani, E., Sun, H., Musinszki, M., Cordeiro, S., Bucci, G., . . . Baukrowitz, T. (2016). A non-canonical voltage-sensing mechanism controls gating in K2p K+ channels. *Cell, 164*, 937–949.
Schröder, W., Seifert, G., Hüttmann, K., Hinterkeuser, S., & Steinhäuser, C. (2002). AMPA receptor-mediated modulation of inward rectifier K+ channels in astrocytes of mouse hippocampus. *Mol. Cell Neurosci., 19*, 447-458.
Seifert, G., Hüttmann, K., Binder, D. K., Hartmann, C., Wyczynski, A., Neusch, C., & Steinhäuser, C. (2009). Analysis of Astroglial K+ Channel Expression in the Developing Hippocampus Reveals a Predominant Role of the Kir4.1 Subunit. *J. Neurosci., 29*, 7474-7488.
Seifert G., H. C. a. S. C. (2018). Diversity of astrocyte potassium channels - An update. *Brain Res Rev, 126*, 26-36.
Sepúlveda, F. V., Cid, L.P., Teulon, J., Niemeyer, M.I.,. (2015). Molecular Aspects of Structure, Gating, and Physiology of pH-Sensitive Background K2P and Kir K-Transport Channels. *Physiol Rev*, 95:179–217.
Soe, R., Andreasen, M., & Klaerke, D. A. (2009). Modulation of Kir4.1 and Kir4.1-Kir5.1 channels by extracellular cations. *Biochim Biophys Acta, 1788*(9), 1706-1713. doi:10.1016/j.bbamem.2009.07.002
Somjen, G. G. (2004). *Ions in the brain : normal function, seizures, and stroke*. Oxford ; New York: Oxford University Press.
Steinhäuser, C., Seifert, G., Deitmer, J.W.,. (2013). Physiology of astrocytes: ionchannels and ion transporters. In *Neuroglia* (pp. 185–196): Oxford University Press.
Tong, X. e. a. (2014). Astrocyte Kir4.1 ion channel deficits contribute to neuronal dysfunction in Huntington's disease model mice. *Nat. Neurosci.*, 17:694.

Traynelis, S. F., & Dingledine, R. (1988). Potassium-induced spontaneous electrographic seizures in the rat hippocampal slice. *J Neurophysiol, 59*(1), 259-276. doi:10.1152/jn.1988.59.1.259
Welling, P. (2016). Roles and Regulation of Renal K Channels. *Ann Rev Physiol, 78*, 415-435.
Wible, B., Tagliatela, M., Ficker, E., & Brown, A. M. (1994). Gating of inwardly rectifying K+ channels localized to a single negatively charged residue. *Nature*, 371:246.
Yang, L., Edvinsson, J., Sackin, H., & Palmer, L. (2012b). Interactions of external K+ and internal blockers in a weak inward-rectifier K+ channel. *J Gen Physiol*, 140:529.
Yang, L., Edvinsson, J., Sackin, H., & Palmer, L. G. (2012a). Ion selectivity and current saturation in inward-rectifier K+ channels. *J.Gen.Physiol.*, 139:145.
Zafar, S., & Jabeen, I. (2018). Structure, Function, and Modulation of gamma-Aminobutyric Acid Transporter 1 (GAT1) in Neurological Disorders: A Pharmacoinformatic Prospective. *Front Chem, 6*, 397. doi:10.3389/fchem.2018.00397
Zeeman, E. C. (1977). *Catastrophe theory : selected papers, 1972-1977*. Reading, Mass.: Addison-Wesley Pub. Co., Advanced Book Program.
Zhou M., X., G., Xie, M., Zhang, X., Schools, G.P., Ma, L., Kimelberg, H.K.,Chen, H. (2009). TWIK-1 and TREK-1 are potassium channels contributing significantly to astrocyte passive conductance in rat hippocampal slices. *J Neurosci, 29*, 8551-8564.
Zuo, D., Chen, K., Zhou, M., Liu, Z., Chen, H. (2017). Kir2.1 and K2P1 channels reconstitute two levels of resting membrane potential in cardiomyocytes. *J Physiol, 595*, 5129–5142.